Solar Energy 316 (2026) 114905

Contents lists available at ScienceDirect

Solar Energy

journal homepage: www.elsevier.com/locate/solener

Adaptive photovoltaic façade for energy efficiency and indoor environmental quality via machine learning based optimization

Sijun Liu [b], Zhaoyang Luo [c], Xiaodong Yang [d], Yudai Liu [e], Yi Zhang [a], Pengyuan Shen [a,*]

[a] Institute of Future Human Habitats, Shenzhen International Graduate School, Tsinghua University, Shenzhen, China
[b] School of Future Design, Harbin Institute of Technology, Shenzhen, China
[c] School of Architecture, Harbin Institute of Technology, Harbin, China
[d] China Construction Eighth Engineering Division, Shanghai, China
[e] East China Architectural Design & Research Institute Co., Ltd., Shanghai, China

A R T I C L E I N F O

Keywords:
Building-integrated photovoltaics
Adaptive façade
Control optimization
Machine learning
Indoor environment
Energy use

A B S T R A C T

This study proposes an adaptive photovoltaic façade system for office buildings in hot summer and warm winter regions, integrating shading, daylighting regulation, and solar power generation within a unified multi-objective optimization framework. Rotatable lamellar units arranged in a layered array enable dual-axis adjustment in response to real-time solar and meteorological conditions. A data-driven XGBoost surrogate model replaces computationally expensive simulations, while NSGA-II drives hourly Pareto optimization across five performance objectives. A Nash bargaining-based decision criterion selects balanced solutions without relying on subjective weighting. Results from representative subtropical climate in Shenzhen, China show the adaptive façade increases annual photovoltaic generation by approximately 15% over fixed louver shading and reduces annual cooling energy consumption by approximately 33% relative to the unshaded baseline. The annual average Spatial Useful Daylight Illuminance (sUDI) reaches 0.89, substantially above the baseline value of 0.66, while spatial Daylight Glare Probability (sDGP) is maintained between 0.15 and 0.21 and the Openness Factor (OF) averages 0.27. The findings in this work demonstrate the feasibility of coordinated multi-objective optimization of energy, daylighting, and visual comfort performance through adaptive photovoltaic façade control.

1. Introduction

The building sector is a major source of global energy consumption and carbon emissions [1]. It accounts for approximately 30–40% of total energy consumption and around 40% of CO_2 emissions, and under current development trends, the share of carbon emissions attributable to the building sector is expected to increase further by 2050 [2,3]. With the acceleration of urbanization, the scale of commercial buildings continues to expand, becoming an important contributor to building energy consumption and carbon emissions [4]. In office buildings, the envelope, particularly the façade system, directly affects solar heat gain and loss, indoor daylighting quality, and air-conditioning loads [5]. Meanwhile, in order to meet the increasing demand for indoor environmental comfort, buildings have become increasingly reliant on active control systems such as air-conditioning and lighting [6]. Therefore, reducing operational energy consumption and carbon emissions while ensuring indoor environmental quality has become a key issue that must be addressed urgently in the field of office buildings.

Against the backdrop of sustainable development, building façades are gradually shifting from traditional static envelope structures toward adaptive systems with environmental responsiveness [7]. Owing to the significant temporal variability of outdoor climatic conditions, static façades are unable to continuously satisfy building performance requirements across different seasons and times of day, whereas adaptive façades can dynamically respond to the luminous environment, thermal environment, and building energy consumption through structural or material-level adjustments [7,8]. On this basis, Building-Integrated Photovoltaics (BIPV), as an important approach for clean energy utilization, has been widely introduced into research on adaptive façades in recent years [9]. Adaptive photovoltaic façades can not only participate in environmental control processes such as shading, daylight modulation, and thermal regulation, but can also simultaneously generate solar power during operation, thereby providing a new technological pathway for reducing building operational energy consumption and carbon emissions [10,11]. Recent studies have further demonstrated

* Corresponding author.
E-mail address: pengyuan_pub@163.com (P. Shen).

https://doi.org/10.1016/j.solener.2026.114905
Received 27 April 2026; Received in revised form 6 July 2026; Accepted 10 July 2026
Available online 20 July 2026
0038-092X/

Nomenclature

Abbreviation

BIPV	Building-Integrated Photovoltaics
CIGS	Copper Indium Gallium Selenide
DA	Daylight Autonomy
DGI	Daylight Glare Index
DGP	Daylight Glare Probability
DHI	Diffuse Horizontal Irradiance
DNI	Direct Normal Irradiance
HVAC	Heating, Ventilation, and Air Conditioning
ML	Machine Learning
OF	Openness Factor
PSO	Particle Swarm Optimization
PV	Photovoltaic
PVSD	Photovoltaic Shading Device
RMSE	Root Mean Square Error
R^2	Coefficient of Determination
sDGP	Spatial Daylight Glare Probability
sUDI	Spatial Useful Daylight Illuminance
TMY	Typical Meteorological Year
UDI	Useful Daylight Illuminance
MPC	Model Predictive Control
NSGA-II	Non-dominated Sorting Genetic Algorithm II
XGBoost	Extreme Gradient Boosting
Sobol	Sobol Sensitivity Analysis

Definition

S1	First-order Sobol index
ST	Total-order Sobol index
Angle1	Solar elevation angle response for shading
Angle2	Solar azimuth angle response for shading
G	Solar irradiance incident on the photovoltaic surface
T	Ambient dry-bulb temperature at a given time
A	Total installed area of photovoltaic panels
E	Photovoltaic electricity generation
t	Time
T_{ref}	Reference temperature, $T_{ref} = 25^{\circ}\mathrm{C}$
μ_{ref}	PV conversion efficiency at the reference temperature
β	Temperature coefficient representing the reduction in efficiency with increasing temperature

that integrating photovoltaic modules into louver-based daylighting systems can simultaneously improve indoor environmental quality and solar energy utilization, while dynamically reconfigurable photovoltaic shading devices offer additional potential for balancing daylight admission, solar heat gain control, and electricity generation [12,13]. Among the climate zones in China, the hot summer and warm winter region faces more severe challenges in controlling building energy consumption and carbon emissions due to its hot and humid summers, cooling-dominated annual loads, and long operating periods of air-conditioning systems [14]. On the one hand, the persistent and intense solar radiation in this region provides considerable potential for photovoltaic power generation; on the other hand, it also significantly increases building cooling loads and the risk of indoor glare. As a result, adaptive photovoltaic façades are both necessary and advantageous under such climatic conditions [1,15].

Existing research on adaptive photovoltaic façades has gradually developed into a research framework centered on façade prototype design, building performance evaluation, and operational control methods. In terms of prototype and configuration exploration, early studies primarily focused on the movement mechanisms and structural forms of adaptive photovoltaic façades. The Adaptive Solar Façade (ASF) system proposed by Nagy et al. is one of the representative works in this field. The system consists of arrayed rhombus-shaped photovoltaic modules and achieves a dynamic response to solar position through dual-axis rotation [16]. Subsequently, research expanded from electromechanically driven tracking mechanisms to material-driven and lightweight configurations. Passive actuation strategies based on the adaptive properties of materials can reduce system operating energy use and improve structural adaptability [17], while foldable and deformable components emphasize structural efficiency and configurational scalability [18,19]. In terms of the integration of shading components, schemes embedding photovoltaic modules into rotatable shading panels/louvers have been widely discussed, and studies have generally indicated that the number of components, their spacing, and their angular range significantly affect the coupling relationship among self-shading, daylight transmittance, and power generation [20]. More recent studies have moved beyond static geometric comparisons toward automated or dynamically reconfigurable louver systems. For example, photovoltaic-integrated daylighting louvers with servo-based slat control have been experimentally shown to improve indoor illumination while maintaining solar generation potential [12], and dynamic photovoltaic shade systems have been examined through multi-objective optimization across multiple climates and configurations [13]. In addition, weather-responsive photovoltaic envelopes with hierarchical slat control strategies have also been proposed for glazed office façades, indicating a growing shift from configuration design toward control-oriented façade operation [21]. Research has also begun to shift toward validation under real or quasi-real conditions, for example, by deploying louver-type photovoltaic façades on existing building elevations and combining them with parametric methods for periodic angle adjustment to examine engineering feasibility and long-term operational performance [22]. Meanwhile, the introduction of emerging photovoltaic technologies and biomimetic concepts has further broadened the possibilities of these systems in terms of efficiency, temperature sensitivity, and configuration generation [23–25].

In terms of building performance evaluation, the research focus has gradually expanded from power generation gains alone to the integrated benefits of power generation, energy consumption, and indoor daylighting performance. Existing studies have demonstrated that dynamic tracking can usually improve power generation potential significantly compared with fixed installation, although the actual benefits are strongly influenced by climate, obstruction conditions, and system posture constraints [26]. Some studies have incorporated building net energy consumption and indoor environmental indicators into the evaluation framework, indicating that adaptive photovoltaic façades have the potential to reduce cooling demand and mitigate excessive solar radiation [16], and that, under certain conditions, power generation optimization and energy consumption minimization may exhibit a certain degree of synergy [27]. From the daylighting perspective, dynamic adjustment and tracking mechanisms have been shown to reduce glare risk, improve useful daylighting, and decrease building operational energy use, while the proportion of energy consumed by the system itself remains relatively low [28,29]. As the number of objectives has increased, multi-objective optimization has gradually become the dominant paradigm. In different climate zones and building types, various studies have incorporated power generation, energy consumption, and visual/thermal comfort indicators into unified optimization frameworks, thereby verifying the advantages of adaptive systems over static façades in terms of overall performance [30,31]. More recently, adaptive BIPV shading systems have been optimized using multi-objective algorithms with simultaneous consideration of electricity generation, building electricity use, spatial daylight autonomy, and daylight glare probability, further extending performance evaluation from static design comparison to adaptive operational optimization [32]. In parallel, machine-learning-assisted BIPV envelope optimization frameworks have shown that surrogate models can substantially reduce computational cost while preserving acceptable prediction accuracy in multi-objective workflows [33,34].

As research has extended from the design stage to the operational stage, control strategies have gradually become a major focus. In recent years, machine learning methods have been employed for tasks such as load prediction, glare prediction, and shading angle control because of their ability to capture nonlinear relationships. Existing studies have shown that data-driven models, including artificial neural networks, can predict building loads, support dynamic louver angle optimization, and reduce glare occurrence as well as lighting energy consumption [35–37]. Comparative studies of multiple models have further shown that data-driven methods can support façade morphing and respond to real-time demands under complex environmental boundary conditions [38]. Recent research has further expanded this direction by applying explainable machine learning to rapid multi-performance prediction of BIPV façades and by developing machine-learning-based adaptive control strategies for photovoltaic shading under dynamic energy and visual comfort objectives [34,39]. In addition, zoning-based adaptive concentrating photovoltaic façade control has also been explored to enhance visual comfort and overall energy benefits, indicating that façade intelligence is gradually evolving from single-angle adjustment toward more refined operational coordination [40].

A synthesis of the existing literature shows that, although adaptive photovoltaic façades have made substantial progress in configurational innovation, integrated performance optimization, and intelligent control, several limitations remain. First, many studies focus primarily on design-stage optimization or on systems with limited motion variables, whereas fewer studies address high-degree-of-freedom adaptive photovoltaic façades under operation-stage, hourly control conditions. Although energy generation, energy use, daylighting, and glare have been studied in different combinations, their coordinated optimization together with view preservation in one unified control framework remains limited. Last but not least, most existing studies commonly rely on Pareto-front generation followed by preference-based or scenario-based selection, while less attention has been given to objective decision rules for selecting balanced operating solutions from the Pareto set without subjective weighting.

To address these gaps, this study proposes an adaptive photovoltaic façade system for office buildings in the hot summer and warm winter climate region. The proposed system employs rotatable lamellar units arranged in a layered array, enabling dual-axis adjustment in response to hourly solar and meteorological variations. A data-driven XGBoost surrogate model is developed to replace computationally expensive simulations, and NSGA-II is used to perform hourly Pareto optimization across five performance objectives, namely photovoltaic power generation, cooling energy use, spatial Useful Daylight Illuminance (sUDI), spatial Daylight Glare Probability (sDGP), and Openness Factor (OF). In addition, a Nash bargaining-based decision criterion is introduced to identify balanced operating solutions from the Pareto set without relying on subjective weighting. Using Shenzhen as a representative subtropical case, this study aims to provide a unified operational optimization framework for adaptive photovoltaic façades that simultaneously improves energy performance, daylighting quality, visual comfort, and view preservation.

2. Methodology

2.1. Adaptive photovoltaic façade system

In the context of building design that places equal emphasis on multi-objective energy conservation and indoor environmental quality, the adaptive photovoltaic façade is positioned as an integrated building envelope system that coordinates shading regulation, daylight admission, and energy harvesting [21,41]. This study introduces a biomimetic approach, translating the adaptive principles of natural systems in regulating light exposure into façade configurations and movement rules. Specifically, biomimetic mechanisms are used to inspire form and motion, a multi-objective evaluation framework is employed to define performance-oriented criteria, and operational control is further used to establish a mapping between façade posture and environmental variation, thereby supporting dynamic optimization.

At the prototype level, this study adopts rotatable lamellar units as the basic components and arranges them in an array across the façade, so as to reconcile the need for modular scalability in large-area applications with the engineering feasibility required for subsequent modeling and controllability.

Fig. 1 illustrates the motion mechanism of the adaptive photovoltaic façade. The system adopts a dual-axis rotation mechanism to achieve a precise response to the incident geometry of solar radiation and introduces a layer-by-layer control strategy at the overall control level. On the basis that each unit is capable of multi-degree-of-freedom adjustment, the components are divided into multiple mutually independent layers according to the differentiated solar exposure conditions along the façade height and their varying influences on the indoor luminous environment. Independent angle settings and response logics are assigned to each layer, enabling targeted regulation of zones at different heights based on their respective irradiation conditions, reflective interference, and shading relationships.

2.2. Typical office space

This study focuses on open-plan office spaces in office buildings. The parameter settings for the office space were determined with reference to relevant studies investigating and analyzing the spatial characteristics of office buildings [42], while also taking into account common structural systems in office buildings and the subdivision requirements of standard unit office spaces. Accordingly, an office space with a floor height of 4.2 m, a window-to-wall ratio of 0.64, a bay width of 9 m, and a depth of 6 m was selected as the research object. Fig. 2 shows the configuration of the adaptive photovoltaic façade. The adaptive photovoltaic façade was designed based on these window dimensions, enabling complete coverage of the window area.

2.3. Evaluation metrics

To enable a closed-loop workflow for façade configuration generation, performance comparison, and control strategy evaluation under a unified objective framework, this study ultimately adopts cooling energy consumption and photovoltaic power generation as the core energy-related indicators. In addition, sUDI, sDGP, and OF are used to characterize daylighting effectiveness, the extent of glare impact, and the degree of visual openness, respectively, thereby establishing an evaluation framework for the coordinated optimization of power generation, energy consumption, the luminous environment, and visual openness.

2.3.1. Energy consumption and production

Cooling energy consumption is used to measure the impact of the façade system on the building's thermal performance and operational energy use, and it is a key indicator for evaluating energy-saving potential and the comparability of different design schemes [43]. By means of dynamic shading, the adaptive photovoltaic façade alters the solar radiation and heat gains entering the indoor space, thereby affecting cooling load demand and the energy consumption of the air-conditioning system.

Photovoltaic power generation is adopted as the primary energy output metric, as it more directly reflects the actual electricity contribution of the adaptive façade than local indicators such as instantaneous

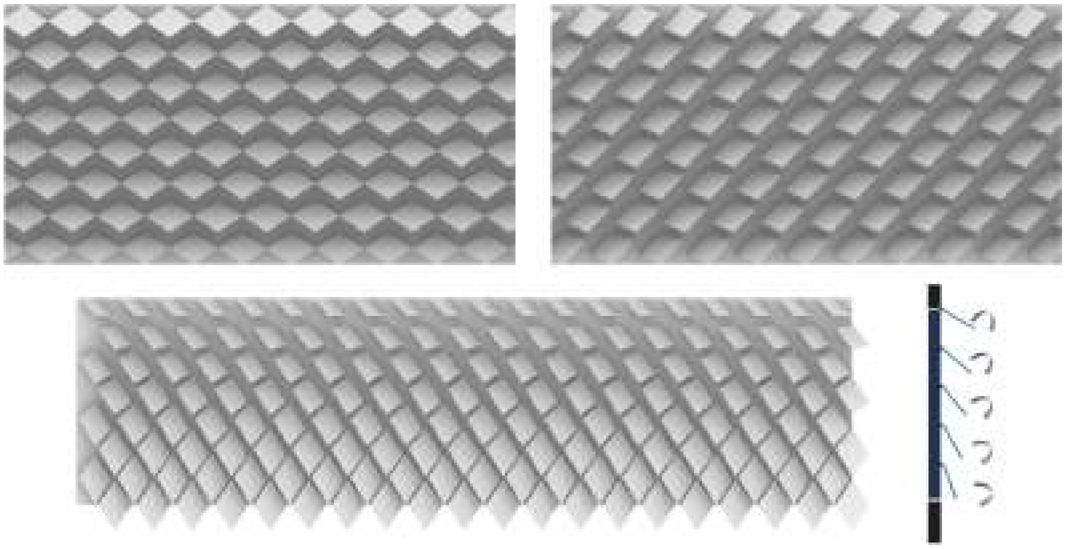

Fig. 1. Adaptive photovoltaic façade movement mechanism.

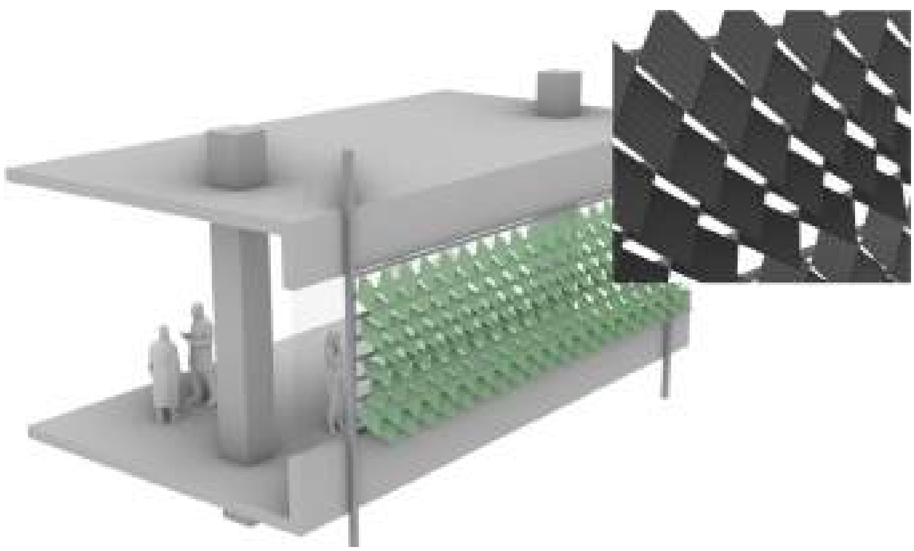

Fig. 2. Adaptive photovoltaic façade setting diagram.

efficiency or peak power [44]. The incident irradiance on each PV module is not simply the horizontal global irradiance but depends on the module's instantaneous orientation, defined by the dual rotation angles θ_1 and θ_2. The effective irradiance on a tilted and rotated module surface is calculated as:

$$G_{\text{eff}}(t) = G_b(t)\cdot\max(\cos\alpha(t), 0) + G_d(t)\cdot\frac{1+\cos\beta}{2} + \rho_g\cdot G_h(t)\cdot\frac{1-\cos\beta}{2}$$

where $G_b(t)$ is the beam (direct) irradiance, $\cos\alpha(t)$ is the cosine of the angle of incidence between the solar ray and the module surface normal (computed from θ_1, θ_2, and the solar position), $G_d(t)$ is the diffuse horizontal irradiance, β is the module tilt angle, ρ_g is the ground reflectance, and $G_h(t)$ is the global horizontal irradiance. The term $\max(\cos\alpha(t), 0)$ ensures that back-irradiance conditions are excluded. In the compact lamellar arrangement adopted in this study, mutual self-shading among adjacent modules further reduces $G_{\text{eff}}(t)$; this effect is evaluated through Ladybug-based ray-tracing irradiance simulation at each time step and for each spatial configuration of the façade.

The PV conversion efficiency is then corrected for module operating temperature using [45]:

$$\eta(T) = \eta_{\text{ref}}\cdot\left[1 - \beta_T\cdot\left(T_{\text{cell}} - T_{\text{ref}}\right)\right]$$

where η_{ref} is the nominal efficiency at the reference temperature $T_{\text{ref}} = 25\,^{\circ}\text{C}$, β_T is the temperature coefficient of efficiency (in K^{-1}), and T_{cell} is the estimated cell operating temperature derived from the ambient dry-bulb temperature and incident irradiance. The electricity output of a single module layer k at time t is:

$$E_k(t) = \eta(T_k(t))\cdot G_{\text{eff},k}(t)\cdot A_k\cdot\Delta t$$

Because the façade adopts a layer-by-layer control strategy, the solar irradiance received by each layer varies significantly along the vertical direction due to differences in tilt angle, self-shading geometry, and solar exposure height. The total façade power generation is therefore obtained by summing across all N independent layers:

$$E_{\text{total}}(t) = \sum\nolimits_{k=1}^{N} E_k(t), \quad E_{\text{annual}} = \sum\nolimits_{t\in\mathcal{T}} E_{\text{total}}(t)$$

This layer-resolved aggregation approach is essential for capturing the spatial heterogeneity of irradiance distribution across the façade height, which would be obscured by a single-module approximation. Together, $E_{\text{cool}} and E_{\text{annual}}$ constitute the two core energy objectives within the multi-objective optimization framework, representing the demand-side and supply-side dimensions of building energy performance, respectively. It should be noted that this irradiance and power aggregation approach captures non-uniform irradiance at the geometric and layer level, reflecting orientation dependent incidence, diffuse and ground reflected components, and inter-module self-shading obtained from ray-tracing simulation. Electrical level effects that can arise under non-uniform irradiance, including mismatch losses between cells or modules, bypass diode activation, and the specific string and MPPT configuration, are not explicitly modeled in this study. The reported PV generation values should therefore be understood as a system level estimate rather than an electrically resolved output, and this is discussed further as a limitation in Section 4.3.

2.3.2. Indoor daylighting performance metrics

Indoor environmental performance indicators are used to constrain and evaluate the façade system from the perspectives of occupant experience and indoor luminous environment quality. In this study, three indicators—sUDI, sDGP, and OF, are selected to represent daylighting adequacy, the spatial extent of glare impact, and visual openness, respectively, with particular emphasis on their ability to characterize the response of dynamic control strategies at the hourly scale.

The quality of indoor daylighting has a substantial influence on occupant comfort and work efficiency [46,47]. sUDI (Spatial Useful Daylight Illuminance) is used to evaluate the proportion of indoor area that falls within the “useful illuminance range” at a given moment. In this study, 100–2000 lx is adopted as the useful illuminance range: values below this range indicate insufficient daylighting and increase the demand for artificial lighting, whereas values above this range are more likely to induce glare and excessive heat gains [48]. The expression is given as follows:

$$sUDI_i = \frac{M_{UDI,i}}{n} \times 100\%$$

where $M_{UDI,i}$ is the number of indoor test points/sensor points with illuminance between 100 and 2000 lx at time step i, and n is the total number of evaluated indoor sensor points.

A well-designed indoor luminous environment can effectively enhance occupants’ visual comfort and psychological well-being; however, if light intensity or distribution is not properly controlled, glare may occur. Glare not only reduces work and learning efficiency but may also exert persistent adverse effects on occupants’ physical and mental health [49]. sDGP (spatial Daylight Glare Probability) is used to describe the spatial extent of glare at a given moment by calculating DGP at multiple viewpoints/test points and determining the proportion exceeding a specified threshold [50]. In this study, DGP $>$ 0.38 is adopted as the threshold for the “disturbing” range to identify glare-affected points, and the proportion of such points at a given moment is defined as the spatial Daylight Glare Probability (sDGP), thereby enabling an assessment of glare-control performance at the spatial scale. The equation is given as follows:

$$sDGP_i = \frac{M_{DGP,i}}{n} \times 100\%$$

where $M_{DGP,i}$ is the number of indoor test points/sensor points with DGP > 0.38 at time step i, and n is the total number of evaluated indoor sensor points.

Outdoor views exert profound physiological and psychological effects on the human body, not only helping to improve health outcomes, but also enhancing occupants’ cognitive performance and spatial satisfaction, alleviating discomfort and stress, and generating positive emotional responses [51]. OF (Openness Factor) is used to quantify the influence of the façade system on the permeability of outward views from the interior, thereby reflecting the balance between glare control and view preservation. In this study, OF is treated as a key constraint indicator and is defined as the proportion of visible openings through the shading system from an indoor observation point (which may be understood as the proportion of effective sightlines), so as to characterize visual openness.

2.4. Machine learning algorithm and meta-modeling

2.4.1. Dataset construction

To replace the high computational cost of performance simulations conducted for each design option and each time period, and to support subsequent optimization iterations, this study develops a data-driven predictive model to rapidly estimate the multidimensional performance of the adaptive photovoltaic façade under different environmental and control conditions. Table 1 illustrates the composition of the dataset, which consists of input features (X) and target variables (Y). On the input side, key variables are extracted from three categories of information—system-intrinsic factors, solar-extrinsic factors, and meteorological boundary conditions—to control the dimensionality of the feature set while preserving physical interpretability and avoiding the introduction of redundancy and noise.

2.4.2. Model selection and setup

In this study, the rapid prediction of façade performance was formulated as a supervised learning regression task. Multiple commonly used regression-based machine learning models were constructed and comparatively evaluated. A unified workflow for data processing, cross-validation, and hyperparameter optimization was applied, and model performance was comprehensively assessed using metrics such as MSE, RMSE, MAE, and R^2, fully illustrating the advantages and disadvantages of each model across multiple indicators, providing a solid basis for subsequent model selection. The hyperparameter settings and performance comparisons of all algorithms are presented in Appendix II. Among them, XGBoost demonstrated relatively low prediction error and a high goodness of fit. Therefore, XGBoost was selected as the predictive model for the five key performance indicators, and its hyperparameter configuration was independently optimized for each target variable to accommodate differences in the response complexity of each indicator.

2.4.3. Model training, validation, and performance

To improve training efficiency and prediction accuracy, five-fold

Table 1
Adaptive photovoltaic surface feature set.

Feature Name	Value Range	Unit	Data Source
Number of horizontal photovoltaic panels (corresponding to module count)	[14,21]	–	Algorithm-generated
Layer-wise values of Angle1 for n independently controlled façade layers (response to solar altitude)	[0,90]	Degree (°)	Algorithm-generated
Layer-wise values of Angle2 for n independently controlled façade layers (response to solar azimuth)	[−90, 90]	Degree (°)	Algorithm-generated
Cosine of the angle between the solar ray and the surface normal of the photovoltaic panel	[−1, 1]	–	Code-calculated
Solar altitude angle	[0,90]	Degree (°)	TMY
Solar azimuth angle	[−180, 180]	Degree (°)	TMY
Global horizontal irradiance	[8]	W/m^2	TMY
Diffuse solar irradiance	[0,400]	W/m^2	TMY

Note: n denotes the number of independently controlled façade layers. Each layer has one Angle1 value and one Angle2 value.

cross-validation and input–output normalization were adopted to enhance training stability [52]. Furthermore, grid search was employed for hyperparameter optimization to identify the optimal combination of parameters for each target variable. Table 2 presents the optimal hyperparameter settings, while the five-fold scatter plots for each performance indicator are provided in Appendix III.

Based on the optimized training framework, the predictive performance of the XGBoost model was further examined for the five key performance indicators. Table 3 summarizes the dataset size and model performance for each target variable. The results indicate that the trained XGBoost models achieved high predictive accuracy and strong goodness of fit across different façade performance indicators, demonstrating their capability to effectively replace the conventional high-cost simulation process.

2.5. Sensitivity analysis

To gain a deeper understanding of how individual input features affect the multi-objective performance of the adaptive photovoltaic façade system, this study conducted a Sobol global sensitivity analysis based on the trained machine learning surrogate models. The analysis systematically quantifies the contribution of each input feature to the variation of model outputs. Specifically, the Sobol method decomposes the total output variance across the design space into individual effects (first-order sensitivity), interaction effects between pairs of inputs (second-order sensitivity), and the total effect of each input (total sensitivity), thereby providing a comprehensive assessment of the influence of different input features on each performance objective [53].

2.6. Multi-Objective optimization and Decision-Making

Based on the identification of underlying mechanisms, this study proposes an adaptive photovoltaic façade control framework that integrates multi-objective optimization with prediction-driven control, with the aim of achieving efficient adaptive regulation of the façade system while simultaneously satisfying multiple objectives, including indoor comfort, energy efficiency, and daylighting quality. The framework employs NSGA-II as the core search algorithm and couples it with the established multi-objective prediction models for collaborative optimization. After obtaining the Pareto solution set, a utility-coordination-based decision criterion is used to select a single deployable control solution.

2.6.1. Geometric optimization

The objective of geometric optimization is to determine the key geometric configurations of the façade system at the design stage, thereby establishing a stable foundation for comprehensive multi-objective performance throughout the year. The optimization variables focus on the geometric configuration of the façade and hierarchical posture control, and their combined effects on power generation, daylighting, glare, view, and energy consumption are evaluated simultaneously within a multi-objective framework. Fig. 3 illustrates the optimization workflow of the geometric parameters of the adaptive photovoltaic façade. Through non-dominated sorting and elitist preservation iterated by NSGA-II within the design space, a well-distributed Pareto-optimal solution set is obtained, providing a rational geometric basis and feasible-domain constraints for subsequent hourly dynamic control.

2.6.2. Hourly dynamic optimization

Hourly optimization is intended to meet the real-time control requirements during the operational stage. Under fixed geometric parameters, control variables such as layer-wise rotation angles are treated as the principal decision variables to achieve multi-objective coordinated regulation according to the solar position and meteorological boundary conditions at the current time step. Leveraging the rapid response capability of the predictive model, the environmental inputs at each time step are mapped to multi-objective performance predictions, and NSGA-II is then used to search for the Pareto solution set for that specific time step. In this way, dynamic trade-offs can be established among sDGP, sUDI, electricity generation, OF, and cooling energy consumption.

2.6.3. Optimization decision-making

NSGA-II outputs a Pareto front solution set; however, engineering deployment requires the selection of a representative compromise solution from the candidate set to generate executable parameter configurations and control commands [54]. In this study, a utility-coordination-based optimal solution selection method derived from the Nash bargaining concept [55] is adopted as the final decision-making criterion. Specifically, the five performance objectives in the Pareto set are regarded as non-hierarchical participants, and a normalized utility function is constructed based on the relative performance of each objective within the candidate set. A unique solution is then selected by maximizing the product of utilities. The overall utility function is defined as follows:

$$NP(x) = \prod_{i=1}^{n} f_i^{\sim}(x)$$

where $f_i^{\sim}(x)$ denotes the normalized utility value of the *i*-th objective. For minimization and maximization objectives, the utility functions are defined as follows, respectively.

For minimization objectives:

$$f_i^{\sim}(x) = \frac{f_i^{\max} - f_i(x)}{f_i^{\max} - f_i^{\min}}$$

For maximization objectives:

$$f_i^{\sim}(x) = \frac{f_i(x) - f_i^{\min}}{f_i^{\max} - f_i^{\min}}$$

This method does not rely on pre-assigned linear weights, nor does it mask the deterioration of any single objective through distance-based aggregation. Instead, by means of a multiplicative mechanism, it imposes a strong penalty on objectives with low utility: if the utility of any one objective is excessively low, the overall utility is substantially reduced. As a result, the final solution achieves a more robust compromise between fairness and overall performance, which is consistent with the engineering requirement of adaptive photovoltaic façade systems

Table 2
Optimal hyperparameter configuration of the XGBoost model.

Hyperparameter	Optimal Value (PV Electricity Generation)	Optimal Value (sUDI)	Optimal Value (sDGP)	Optimal Value (OF)	Optimal Value (Cooling Energy Consumption)
n_estimators	1000	700	700	1000	700
learning_rate	0.02	0.15	0.15	0.02	0.15
max_depth	4	7	7	4	9
min_child_weight	6	1	1	6	3
subsample	0.5	0.7	0.7	0.5	0.7
colsample_bytree	0.9	0.9	0.9	0.7	0.9

Table 3
Sample size of machine learning models and model performance table.

Dataset	Photovoltaic power generation model	sUDI model	sDGP model	OF model	Cooling energy consumption model
Total dataset size	4000	1000*3650	1000*3650	4000	1000*3650
MSE	0.018644	0.000522	0.000306	0.000243	0.016585
RMSE	0.136545	0.022845	0.017508	0.015439	0.128784
MAE	0.096264	0.015816	0.010409	0.012219	0.048731
R^2	0.966558	0.986463	0.980874	0.957426	0.996438

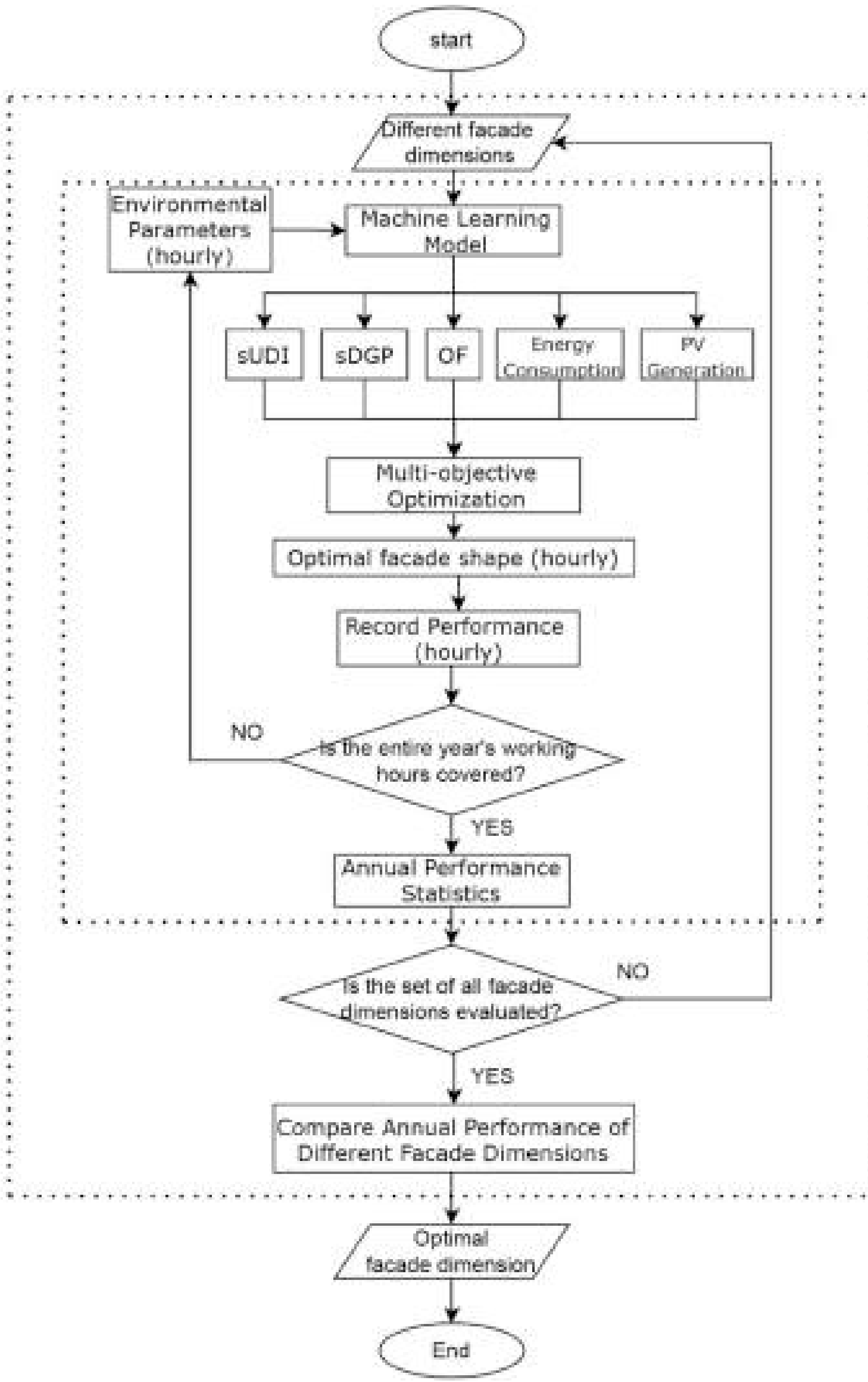

Fig. 3. Flowchart of adaptive photovoltaic façade geometric parameter optimization.

that no objective should be compromised.

3. Results and analysis

3.1. Sensitivity analysis results

As shown in Fig. 4, which presents the first-order Sobol sensitivity indices, and Fig. 5, which presents the total-order Sobol sensitivity analysis results, the mechanisms through which different categories of parameters affect each performance objective differ markedly. Overall, façade-related parameters, solar-position parameters, and meteorological parameters jointly determine façade performance; however, their effect magnitudes and influence pathways are not the same.

Façade-related parameters include the photovoltaic panel module and the rotation angle of each layer. Their overall contributions are relatively limited in the first-order sensitivity analysis, but they increase substantially in the total-order sensitivity analysis, exhibiting the typical characteristics of parameters with weak main effects but strong interaction effects. This indicates that façade-related parameters do not directly determine the system performance level; rather, they enable fine-grained regulation of radiation reception, shading rhythm, and spatial distribution through synergistic interactions with solar-position and meteorological parameters. Specifically, the photovoltaic panel module primarily amplifies the system response to changes in external conditions by altering geometric repetition and shading rhythm, whereas the rotation-angle parameters are manifested more as local geometric adjustments and play differentiated regulatory roles across different performance objectives.

Both solar altitude and solar azimuth exhibit significant contributions in terms of both first-order and total-order sensitivity across multiple performance objectives, indicating that solar-position parameters not only directly determine the angle of solar incidence and light path, but also affect shading relationships and view distribution through interactions with façade geometric parameters. Compared with meteorological parameters, solar-position parameters show greater variation in sensitivity across different objectives. In daylighting- and glare-related indicators, their interaction effects are particularly pronounced; in energy-consumption and electricity-generation objectives, they are manifested more as geometric constraint factors acting jointly with radiation conditions. These results suggest that solar position is not a single controllable variable, but rather an important intermediary linking the external environment with the façade regulation mechanism.

Meteorological parameters generally show high and stable contributions in the first-order sensitivity analysis, and they constitute significant main effects for most performance objectives, including daylighting, glare, photovoltaic power generation, and cooling energy consumption. This indicates that overall system performance is governed first and foremost by external radiation conditions, with the meteorological environment providing the fundamental driving background for performance variations in the photovoltaic façade. In the total-order sensitivity results, meteorological parameters still maintain high contributions, indicating that they not only directly affect performance outputs, but also amplify the effects of geometric regulation through coupling with solar-position and façade-related parameters, thereby serving as a prerequisite for the effectiveness of all types of design variables.

Taken together, the multi-objective performance of the adaptive photovoltaic façade system is not dominated by any single parameter; rather, it is jointly determined by a multi-level coupling mechanism in which the meteorological environment provides the fundamental driving force, solar position imposes geometric constraints, and façade-related parameters enable structural regulation. These findings indicate that, in subsequent multi-objective optimization, isolated adjustment of any single parameter should be avoided. Instead, module configuration and angle-control strategies should be coordinated systematically under the joint constraints of environmental conditions and solar position.

3.2. Optimization process and results analysis

After clarifying the hierarchical effects of different parameter categories on system performance, this study proceeded to conduct a multi-objective optimization to simultaneously improve photovoltaic power generation, the indoor luminous environment, and cooling energy consumption. All objective functions were normalized. The convergence behavior of the algorithm and the quality of the obtained solution set were evaluated by observing the evolution of both the objective space and the decision space during population evolution.

3.2.1. Convergence analysis

With the progressive advancement of the iterations, the objective values, which were initially discretely distributed in the normalized space, gradually converged toward high-performance regions, with a

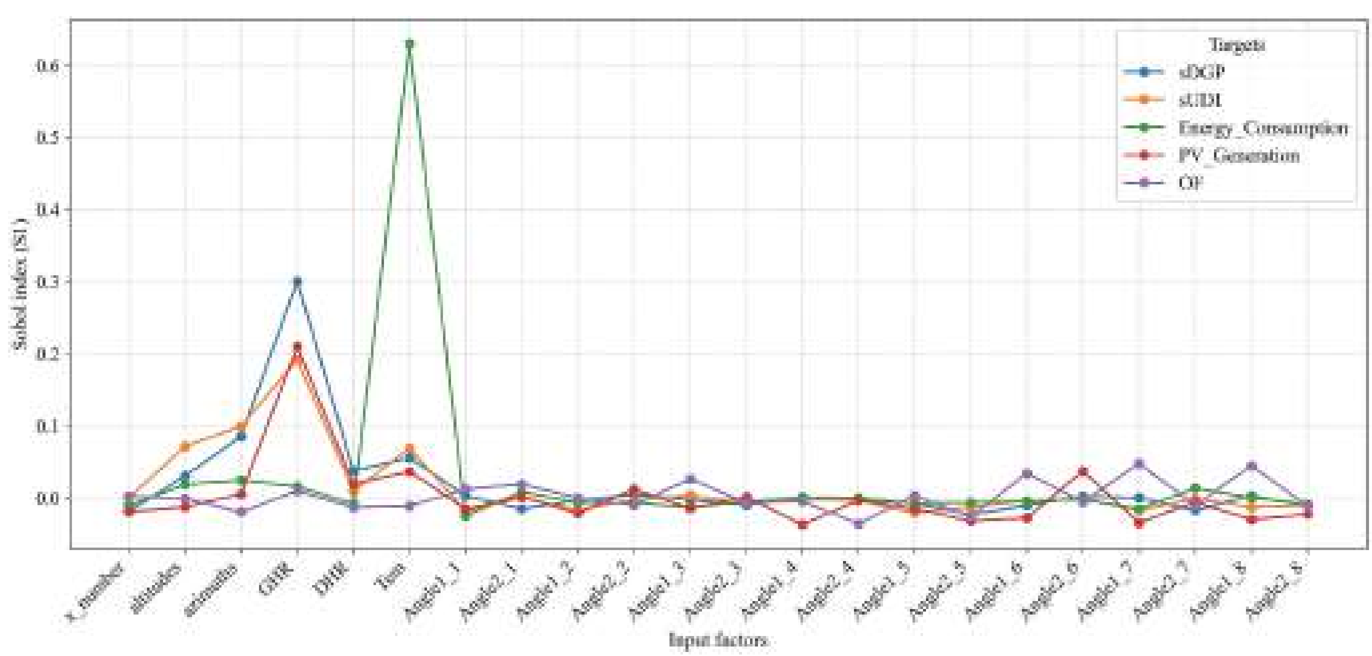

Fig. 4. Comparison of Sobol S1 across targets.

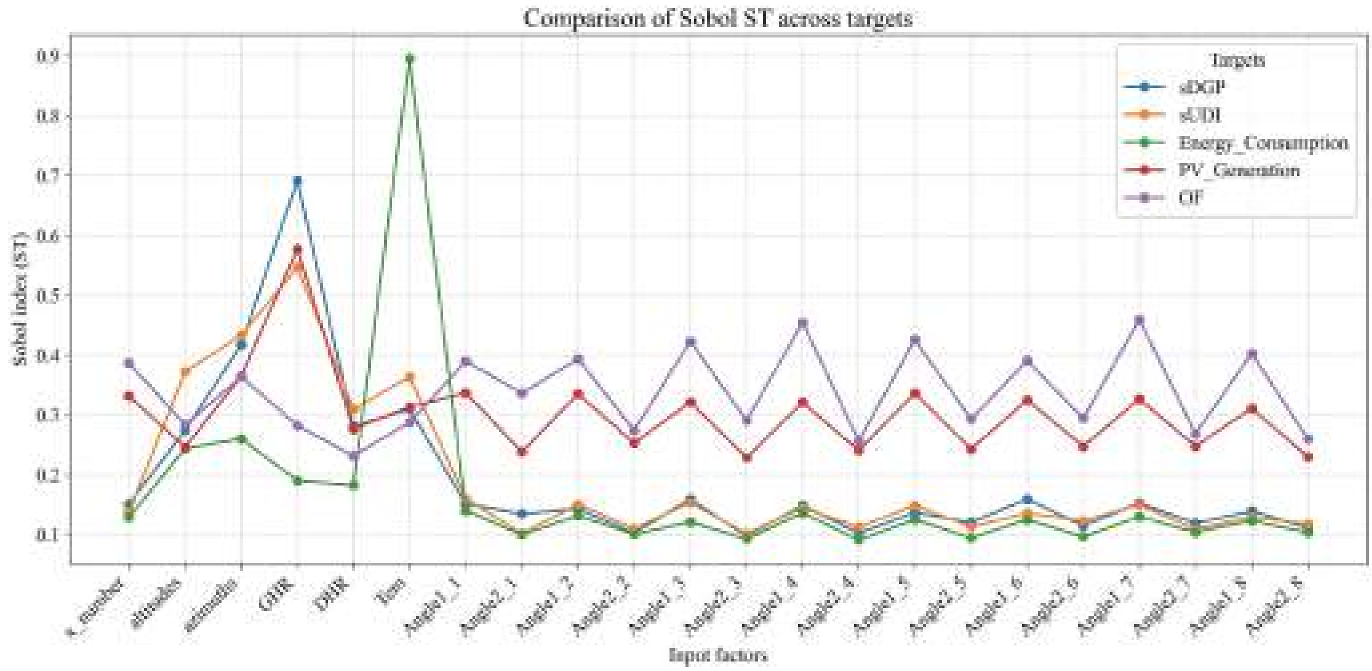

Fig. 5. Comparison of Sobol ST across targets.

marked reduction in distribution range. The solution set evolved from the random and disordered state observed at the early stage into a stable aggregation along the Pareto front, while the trade-off relationships among different objectives became increasingly clear. Meanwhile, the high-dimensional decision variables, which were initially fluctuating and scattered, gradually formed relatively stable value ranges, and the variable combinations corresponding to high-performance solutions became progressively concentrated. This indicates that, while maintaining population diversity, the algorithm continuously improved the overall quality of the solutions, effectively identified superior solution structures, and achieved a stable approximation to the Pareto front.

3.2.2. *Optimization result overview*

After obtaining the Pareto solution set, this study adopted a comprehensive evaluation method based on the Nash utility product to rank and stratify the candidate solutions. By calculating the product of the normalized objective values of each solution and partitioning the solution set according to quartile-based stratification, high-efficiency solutions with balanced performance across multiple objectives could be identified intuitively.

Fig. 6 illustrates the distribution of solutions evaluated by the Nash utility product across different objectives. The results show that solutions with high Nash utility are mainly distributed near the Pareto front and maintain relatively high performance across multiple objective dimensions, whereas low-utility solutions are generally disadvantaged because one or a few objectives perform poorly. The representative solution selected on the basis of this evaluation not only preserves Pareto optimality but also achieves a balanced performance among multiple objectives, thereby serving as the baseline scheme for the subsequent analysis of façade morphology and performance comparison.

3.3. *Façade configuration analysis*

The optimization results are reflected not only in the performance metrics but also in the specific geometric adjustment patterns of the façade. Therefore, this section analyzes the variation characteristics of the adaptive photovoltaic façade from a morphological perspective, with a focus on the angle-change patterns at intra-day, seasonal, and annual scales, in order to reveal the control logic of the system under multi-objective constraints.

3.3.1. *Typical day analysis*

The spring equinox, summer solstice, autumn equinox, and winter solstice were selected as representative days, and 9:00, 13:00, and 17:00 were chosen as key moments for intra-day comparative analysis. Table 4 shows the façade morphology at different times on these representative days. Overall, the façade exhibits a general pattern of “converging at noon and opening in the morning and late afternoon.” During the morning and late-afternoon periods, the unit tilt angles are relatively large to accommodate low solar altitude conditions and to improve daylighting and outward view. Around noon, the tilt angles decrease to suppress excessive solar radiation and reduce indoor cooling loads.

At the seasonal scale, the façade is more compact under summer-solstice conditions, reflecting a shading response to a high-radiation environment. Under winter-solstice conditions, the façade becomes relatively open, which is conducive to admitting solar radiation and enhancing passive heating. The spring-equinoctial and autumn-equinoctial configurations fall between these two extremes. Spatially, the units at different height levels exhibit a gradient distribution: the upper-level units have smaller angles, the middle-level units are moderate, and the lower-level units have larger angles. In this way, a clearly differentiated façade structure is formed, with distinct functional roles in shading, power generation, daylighting, and view provision. Although the morphological generation of the adaptive photovoltaic façade in this study was primarily driven by performance indicators such as photovoltaic power generation, the indoor luminous environment, and cooling energy consumption, its final configuration is an organized form with an inherent order produced through multi-objective trade-offs. Under this performance-oriented generative logic, the tilt angles and opening degrees of units at different heights vary continuously and gradually, creating a function-oriented spatial transition. As a result, while meeting performance requirements, the façade also presents a clearly layered elevation rhythm, thereby avoiding the monotony associated with mechanical repetition.

To better illustrate the relationship between the adaptive photovoltaic façade and environmental variables, comparative plots were developed by dividing the façade into upper, middle, and lower zones according to elevation position. Angle1 was used to characterize the

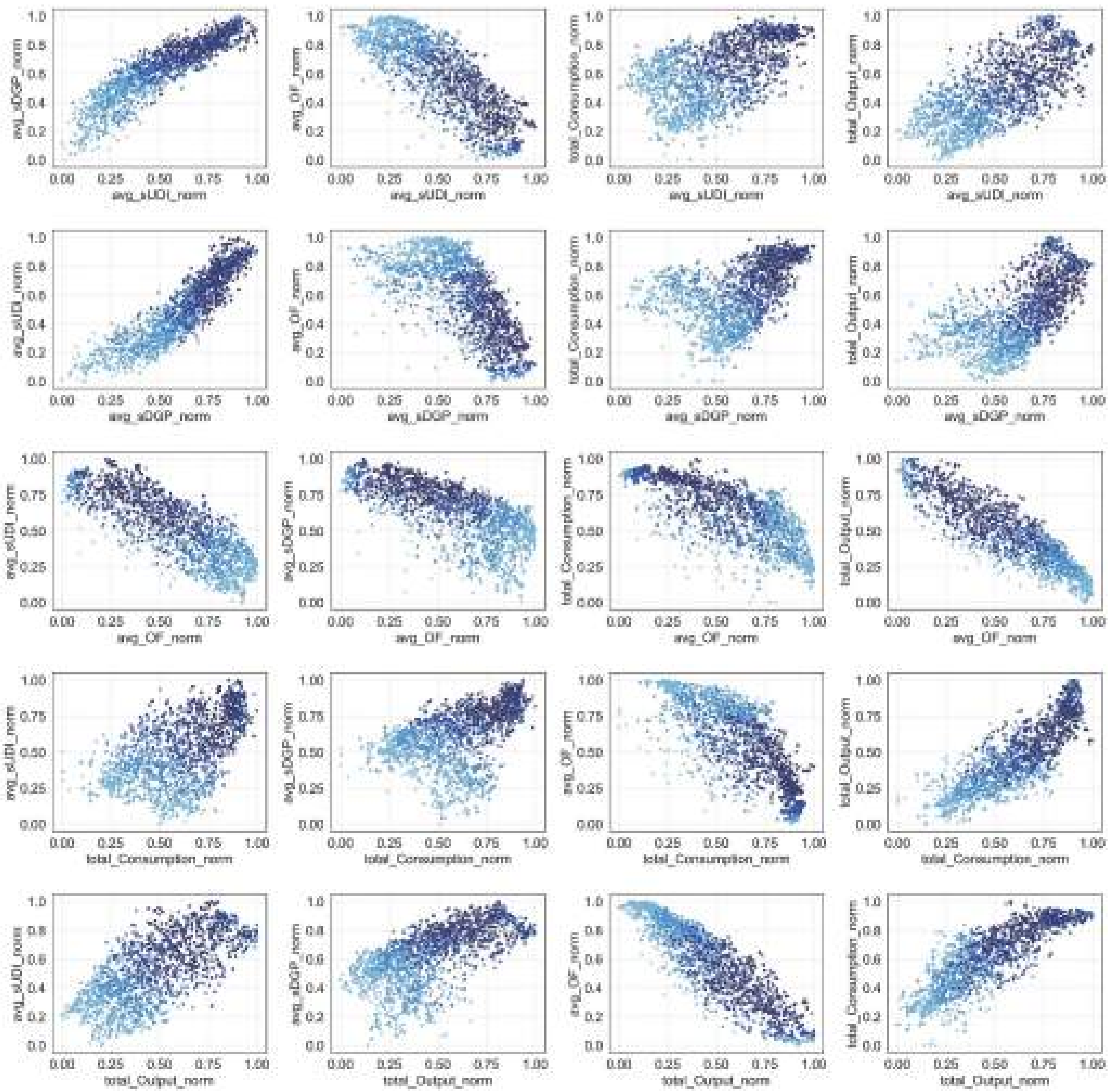

Fig. 6. Scatter plot of pairwise relationships among metrics stratified by Nash utility product values.

shading and light-transmitting state of the façade, whereas Angle2 was used to represent the east–west deflection direction, thereby enabling an evaluation of the system's integrated adaptability to variations in solar altitude and azimuth.

Fig. 7 and Fig. 8 show the relationships of Angle1 and Angle2 with environmental variables, respectively. Angle1 mainly reflects variations in the opening and closing state of the components, with its control primarily aimed at responding to changes in solar altitude and radiation intensity. Overall, the upper- and middle-level components tend to converge under high-radiation conditions so as to enhance shading performance while also accommodating photovoltaic utilization. In contrast, the lower-level components maintain a relatively higher degree of openness, indicating that their regulation serves not only shading purposes but also simultaneously considers daylighting, outward view, and indoor comfort requirements. Angle2 mainly reflects variations in the deflection direction of the components, and its function is more specifically associated with adapting to the dynamic changes in solar azimuth throughout the day. As the sun moves from east to west, the components adjust their orientation through deflection to improve their adaptability to solar incidence directions at different times of day. Accordingly, this angle is more closely associated with directional correction than with opening-amplitude adjustment. Overall, the two angles assume different roles in opening control and directional correction, respectively, and generate differentiated responses across height levels, thereby jointly enabling the photovoltaic façade to achieve a dynamic balance among shading, daylighting, power generation, and indoor environmental quality.

3.3.2. *Annual analysis*

Fig. 9 presents a heat map of the monthly mean values of the façade

Table 4
Comparison of façade configuration at different times of typical days.

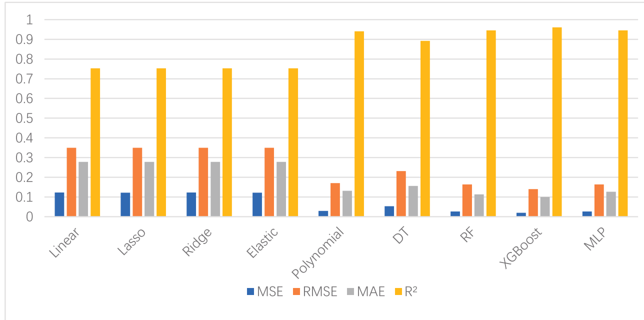

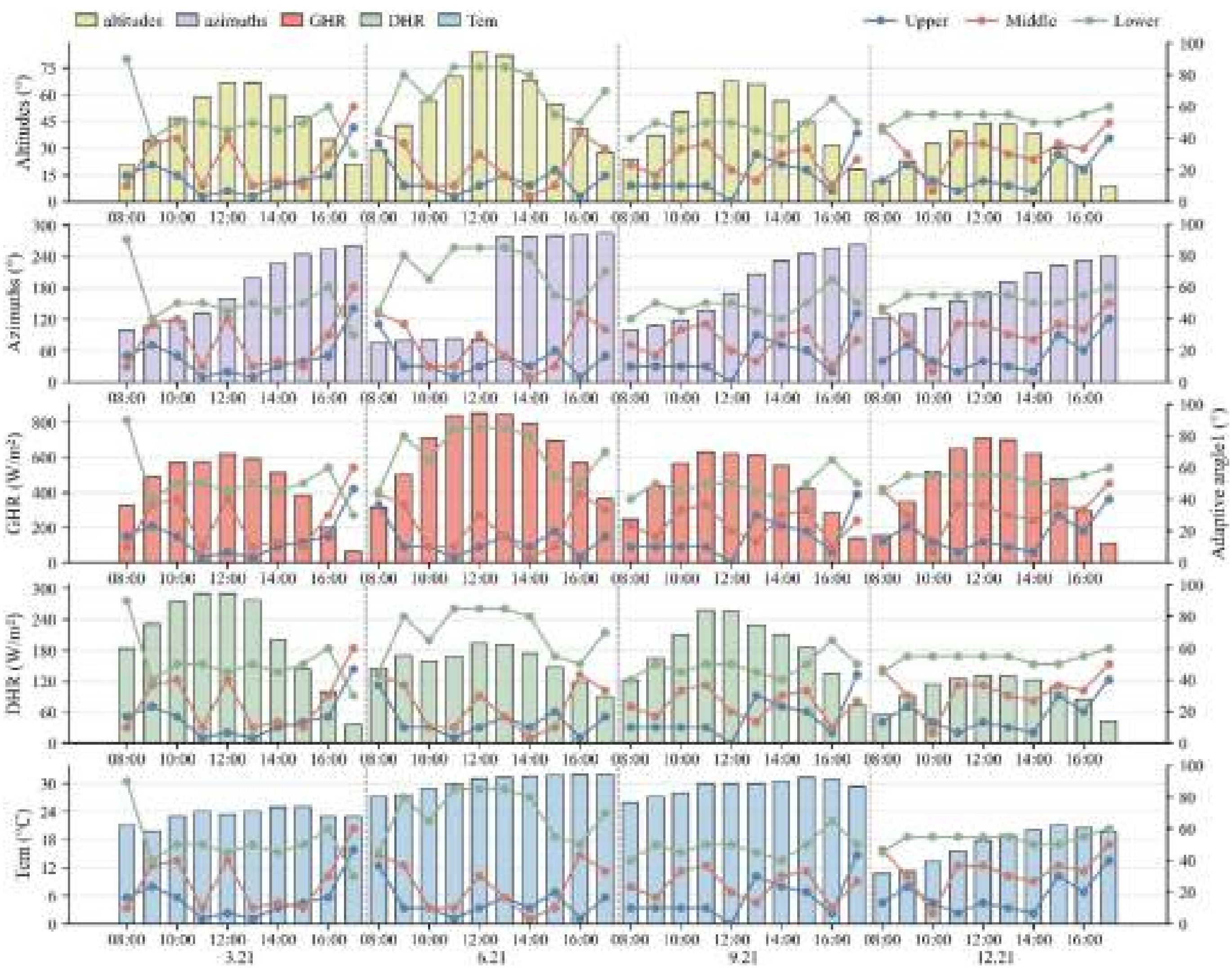

Fig. 7. Typical day Angle1 with climate variables.

rotation angles, namely Angle1 (response to solar altitude) and Angle2 (response to solar azimuth).

The annual distribution of Angle1 indicates a stable pattern during 8:00–17:00, characterized by making smaller angles at midday and larger angles in the morning and late afternoon. A low-angle interval is formed between 11:00 and 13:00, reflecting the façade's intra-day adaptive shading response to variations in solar altitude. A clear functional differentiation is observed across height levels. The upper zone adopts smaller angles to enhance high-level shading and photovoltaic power generation efficiency; the middle zone balances shading and daylighting; and the lower zone maintains larger angles, particularly in the morning and late afternoon, to prioritize outward view and visual comfort. Seasonally, higher angles in winter are conducive to admitting daylight, whereas lower midday angles in summer help

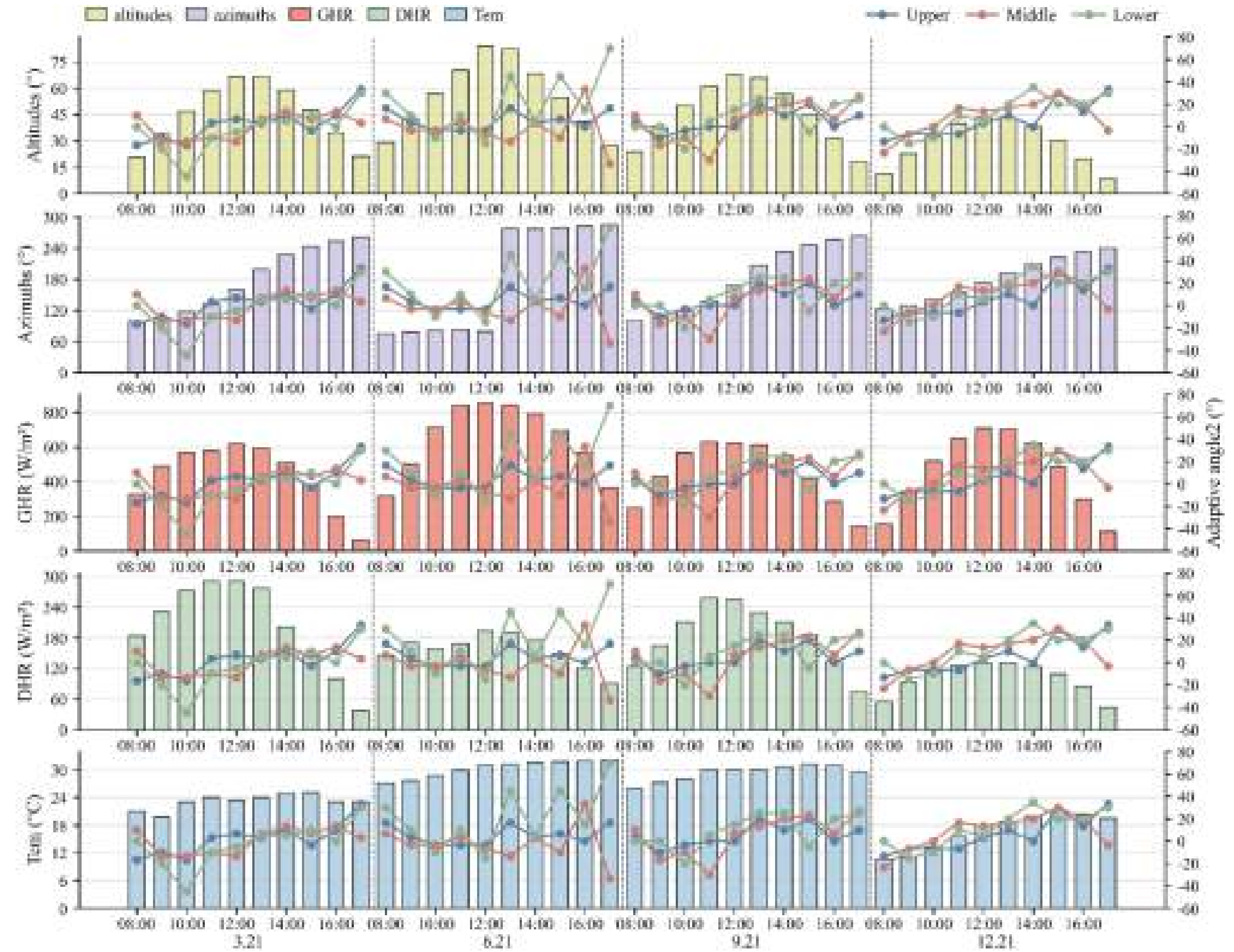

Fig. 8. Typical day Angle2 with climate variables.

suppress solar radiation and reduce cooling loads.

Angle2 exhibits an intra-day deflection pattern consistent with the solar azimuth: it is negative and eastward in the morning, shifts to positive and westward in the afternoon, and approaches zero at noon, when it tends toward due south. This angle works in coordination with Angle1 to respond to high-angle direct solar radiation. The lower zone shows a more moderate deflection range so as to reduce interference with outward view, whereas the middle and upper zones adopt more active deflection strategies to improve shading performance and photovoltaic power generation. Taken together, the annual distributions of Angle1 and Angle2 suggest that the photovoltaic façade develops a clear hierarchical regulation strategy over the façade height: the lower zone prioritizes outward view and occupant comfort, the middle zone balances shading and daylighting, and the upper zone primarily responds to solar radiation while enhancing photovoltaic power output.

3.4. Typical day performance evaluation

To investigate the adaptability of the façade under different environmental conditions, this study comparatively analyzes the relationships between the façade performance indicators, including sUDI, sDGP, OF, cooling energy consumption, and photovoltaic power generation. The analysis focuses on revealing how the façade responds to changes in season, climate, and radiation conditions. The dataset covers hourly samples collected on four representative days: the spring equinox, summer solstice, autumn equinox, and winter solstice.

Fig. 10 and Fig. 11 illustrate the relationships between the façade performance indicators and environmental variables. Overall, the façade system exhibits pronounced and differentiated responses under varying external environmental conditions: some performance indicators are primarily governed by the seasonal climatic background, whereas others are more sensitive to solar radiation and solar position. sUDI is mainly influenced by the seasonal climatic background, particularly air temperature, whereas sDGP is more sensitive to radiation intensity, indicating that glare risk is primarily driven by solar radiation intensity. OF is negatively correlated with solar altitude and radiation-related indicators, suggesting that the façade tends to converge under high-radiation conditions to enhance shading, thereby reducing openness. Cooling energy consumption shows the strongest positive correlation with temperature, indicating that cooling loads are mainly controlled by the external thermal environment. Photovoltaic power generation is positively correlated with total solar radiation, indicating that photovoltaic output is affected not only by solar radiation but also by the thermal state of the components.

3.5. Annual performance evaluation

To evaluate the annual performance of the proposed system in a

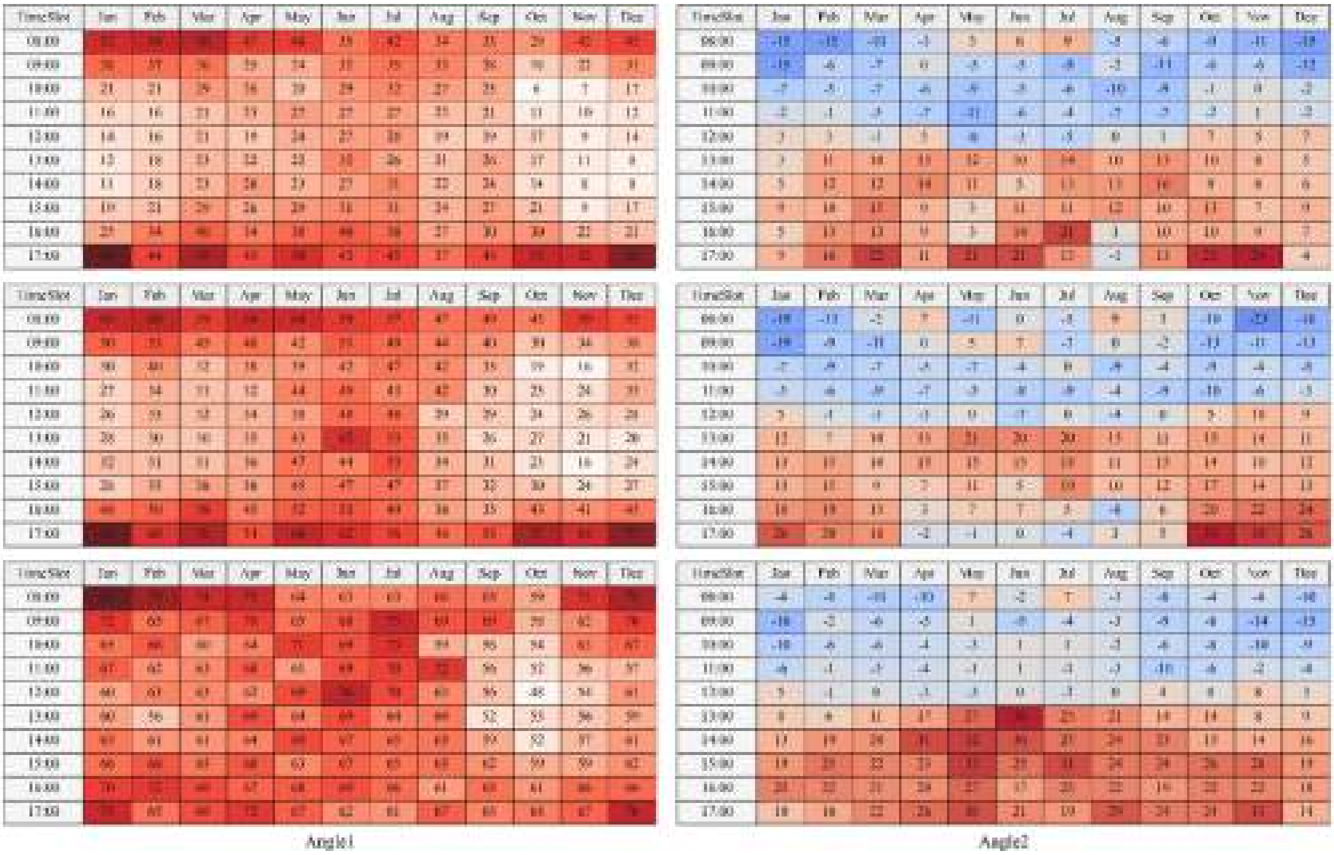

Fig. 9. Heatmap of the average values of the façade angle for each month.

consistent manner, four comparison cases were considered under the same office-space condition: no-façade, photovoltaic louver shading, fixed-angle photovoltaic façade, and adaptive photovoltaic façade. The no-façade case was used as the reference, while the other three cases were compared under identical geometric conditions. Specifically, in all façade-integrated cases, the PV modules were designed to fully cover the window area, and the key geometric parameters, including PV coverage, element spacing, shading depth, and angle constraint range, were kept consistent. In particular, the fixed-angle photovoltaic façade refers to the optimal static angle configuration determined through year-round optimization of the adaptive façade angle variables, and this fixed setting was then used throughout the year for comparison. Therefore, the differences in annual performance among these cases primarily reflect the influence of different operation and control strategies rather than geometric discrepancies. Based on this unified comparison framework, the following sections present the annual energy and indoor environmental performance of the different cases.

3.5.1. *Energy performance evaluation*

Fig. 12 compares the monthly cooling energy consumption and photovoltaic power generation of the adaptive photovoltaic façade. In terms of overall annual electricity generation, the adaptive photovoltaic façade demonstrates a consistent advantage in photovoltaic performance. The no-façade case yields an annual electricity generation of 0 kWh, whereas the annual cumulative electricity generation of the photovoltaic louver shading, fixed-angle photovoltaic façade, and adaptive photovoltaic façade is 3590.16 kWh, 4046.17 kWh, and 4131.50 kWh, respectively. Compared with the photovoltaic louver shading scheme, the adaptive photovoltaic façade increases annual electricity generation by approximately 15.1%, of which the optimized fixed-angle configuration contributes about 12.7%, while hourly dynamic angle adjustment provides a further improvement of about 2.1%. It should be noted that the fixed-angle photovoltaic façade refers to the optimal static angle configuration determined through annual optimization and therefore already represents an optimized photovoltaic arrangement. From the monthly distribution, the adaptive photovoltaic façade achieves higher electricity generation than the fixed-angle photovoltaic façade in most months of the year, with a more pronounced advantage during the transitional seasons, when solar altitude varies substantially. Under the high solar altitude conditions in summer, the difference between the two decreases. In addition to the improvement in photovoltaic electricity generation, the advantage of adaptive angle adjustment is also reflected in the coordinated enhancement of overall façade performance, including lower cooling energy consumption, improved glare control, and better visual openness.

In terms of cooling energy consumption, the no-façade case records the highest annual cooling energy consumption, at 3980.07 kWh. The annual cooling energy consumption of the photovoltaic louver shading, fixed-angle photovoltaic façade, and adaptive photovoltaic façade is 2878.60 kWh, 2805.35 kWh, and 2650.34 kWh, respectively. Using the no-façade case as the reference, all three shading schemes significantly reduce cooling energy consumption, among which the adaptive photovoltaic façade achieves the highest energy-saving rate, outperforming the fixed-angle photovoltaic façade and the photovoltaic louver shading scheme. This demonstrates that it delivers the best annual energy-saving performance. In terms of monthly variation, the adaptive photovoltaic façade exhibits the lowest or nearly the lowest cooling energy consumption in most months, with the most significant advantage occurring during the high-load summer months. During the transitional seasons, it maintains a stable energy-saving performance. In winter, the differences among the schemes become smaller, although its energy consumption control remains relatively stable.

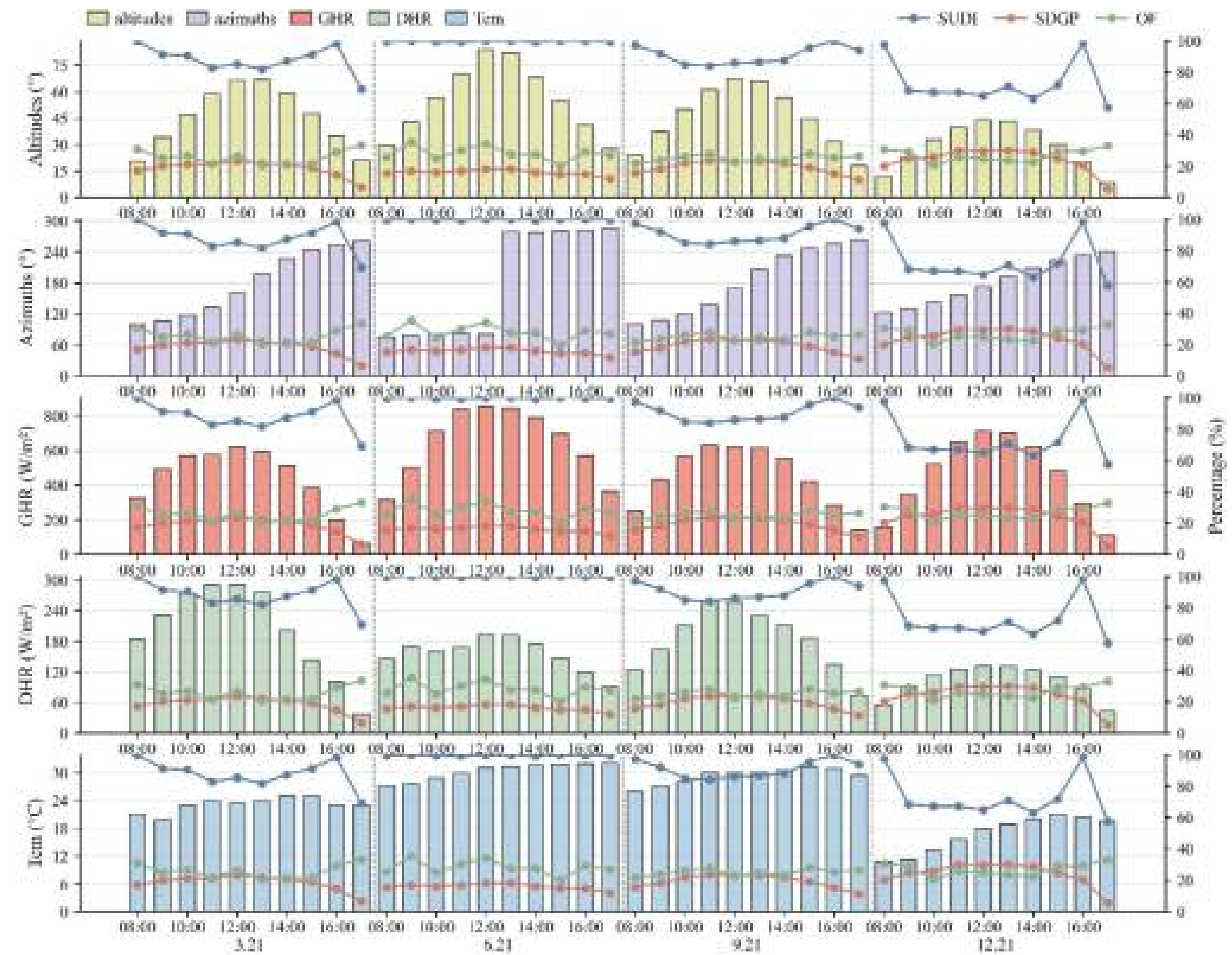

Fig. 10. Typical day façade indoor environment performance with climate variables.

3.5.2. Indoor environment performance evaluation

Fig. 13 presents a monthly comparison of the indoor luminous environment of the adaptive photovoltaic façade throughout the year. In terms of sUDI, the no-façade case shows the lowest annual average value. The fixed-angle photovoltaic façade and the adaptive photovoltaic façade achieve annual average sUDI values of approximately 0.85 and 0.89, respectively, while the photovoltaic louver shading performs best, reaching approximately 0.90. Compared with the no-façade case, the fixed-angle and adaptive photovoltaic façades improve sUDI by approximately 28.8% and 34.8%, respectively, indicating that shading and daylight-regulating components can substantially enhance the effective use of natural daylight. Among the three shading schemes, photovoltaic louver shading performs slightly better in terms of the single sUDI metric, exceeding the adaptive scheme by approximately 1.1%; however, this advantage is limited to this single daylighting indicator. From the monthly perspective, the adaptive photovoltaic façade achieves higher sUDI than the fixed-angle photovoltaic façade in every month of the year, with a more pronounced advantage under the low solar altitude conditions in winter. In summer, all shading schemes maintain relatively high sUDI levels, and the difference between the adaptive photovoltaic façade and the photovoltaic louver shading becomes small.

In terms of sDGP, the no-façade case records the highest values, with glare risk increasing markedly under low solar altitude conditions in winter. After shading devices or photovoltaic façades are introduced, sDGP decreases significantly in all cases, among which photovoltaic louver shading shows the strongest overall glare suppression effect. The sDGP of the adaptive photovoltaic façade ranges from 14.84% to 21.31% and is generally lower than that of the fixed-angle photovoltaic façade, indicating that dynamic adjustment is more effective in reducing direct solar penetration. In summer, all three shading schemes substantially reduce glare probability, and the adaptive photovoltaic façade performs better overall than the fixed-angle scheme. From the monthly distribution, the adaptive photovoltaic façade reduces sDGP by approximately 2 percentage points relative to the fixed-angle scheme in winter, demonstrating that dynamic adjustment can more effectively mitigate direct sunlight under low solar altitude conditions. During summer (June–August), all three shading schemes significantly reduce the probability of glare occurrence. Compared with the no-façade case, the adaptive photovoltaic façade consistently lowers sDGP by approximately 8.94–10.74 percentage points, and overall outperforms the fixed-angle photovoltaic façade.

For OF, the no-façade case maintains a constant annual value of 1.00. The annual OF values of the fixed-angle photovoltaic façade and photovoltaic louver shading are 0.22 and 0.23, respectively, indicating a relatively high degree of view obstruction. By contrast, the adaptive photovoltaic façade increases the annual average OF to approximately 0.27, demonstrating a better balance between shading control and visual

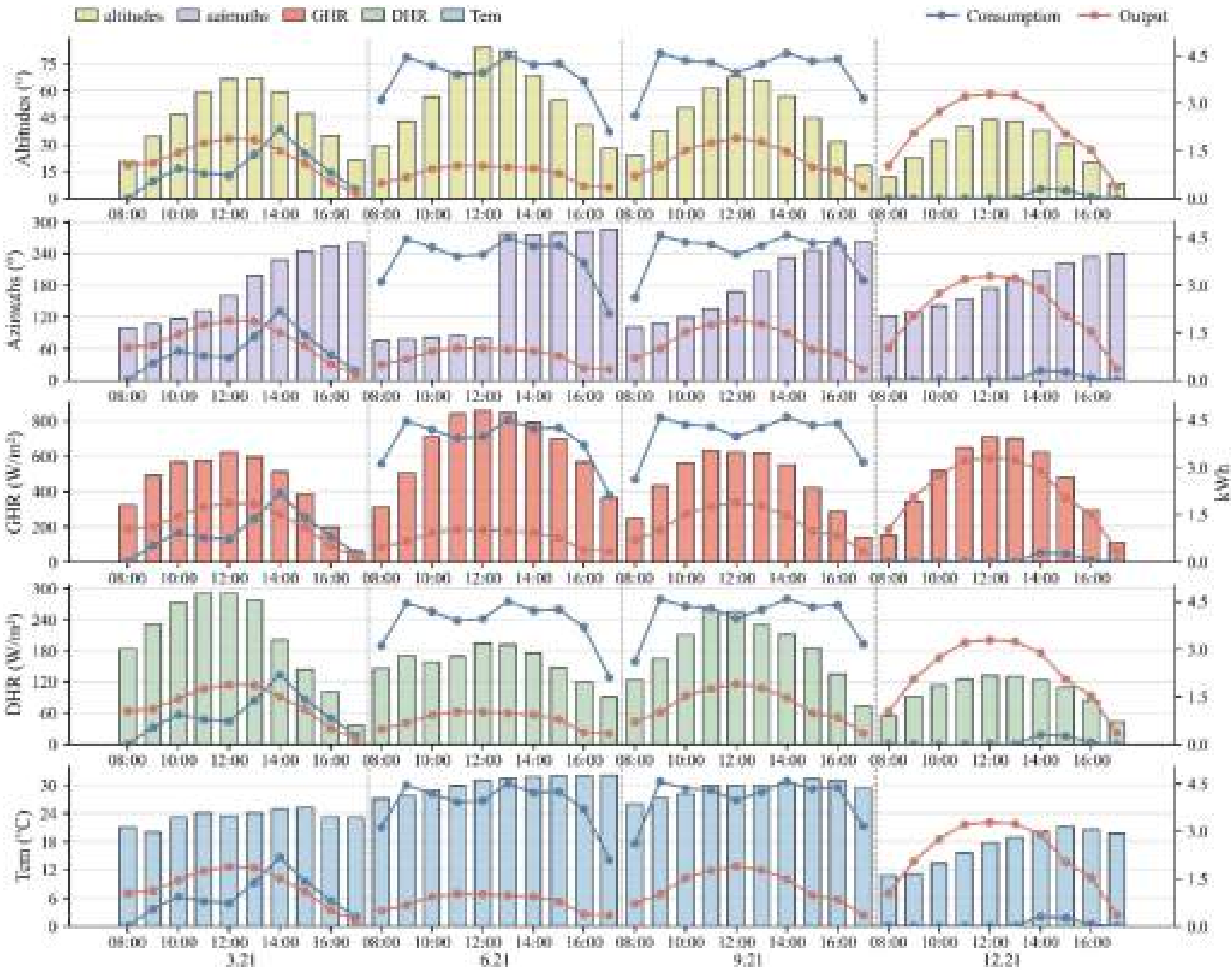

Fig. 11. Typical day façade energy performance with climate variables.

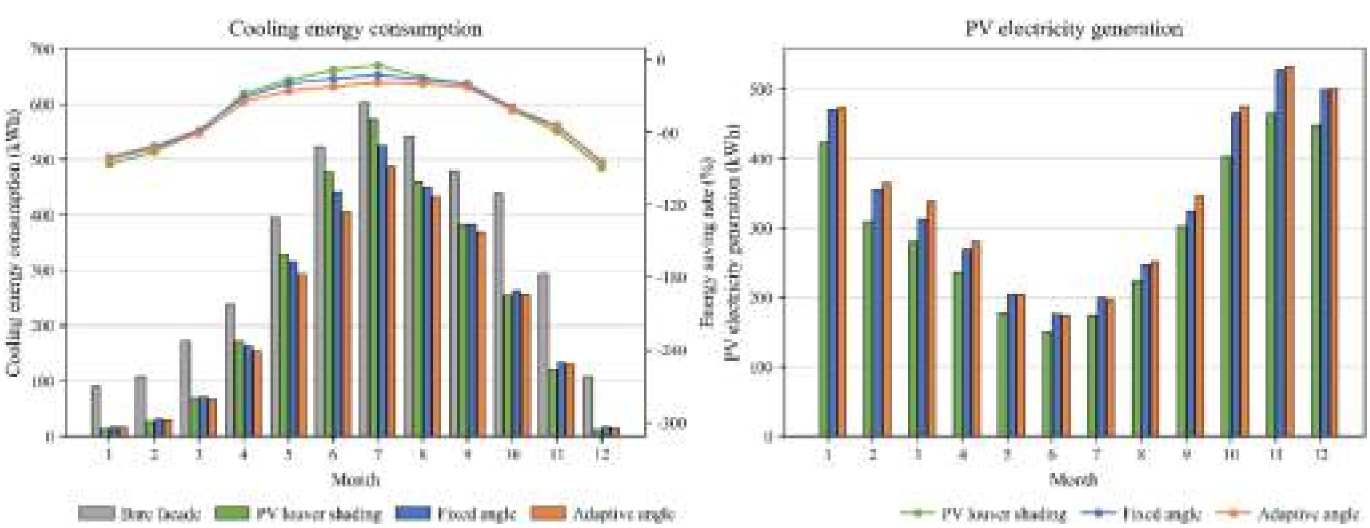

Fig. 12. Monthly comparison of energy performance.

openness. From the monthly distribution, the OF of the adaptive photovoltaic façade remains stable within the range of 0.25–0.29 and is consistently higher than that of both the fixed-angle photovoltaic façade and photovoltaic louver shading throughout the year. Even during

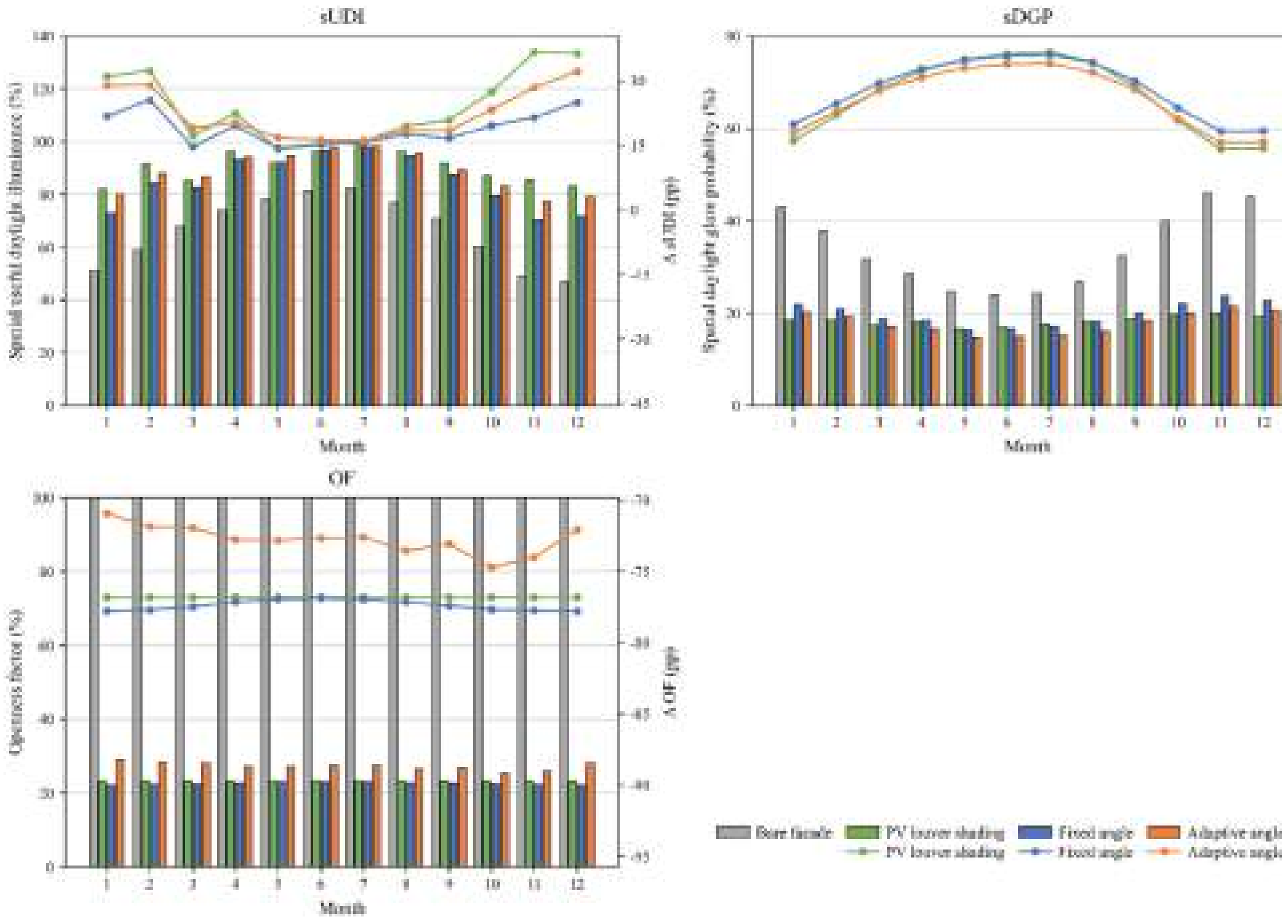

Fig. 13. Monthly comparison of Indoor environment performance.

summer (June–August), when shading demand is relatively high, the adaptive system is still able to maintain a comparatively high level of visual openness, thereby avoiding prolonged and excessive shading.

4. Discussions

4.1. Interpretation of environmental performance of the proposed system

The results demonstrate that the proposed adaptive photovoltaic façade achieves simultaneous improvement across energy, daylighting, and visual comfort objectives, a finding that aligns with but extends beyond previous work in the field. The 15.1% increase in annual photovoltaic generation relative to fixed louver shading is consistent with prior studies reporting that dynamic tracking mechanisms enhance energy capture compared with static configurations, particularly during transitional seasons when solar altitude varies substantially. Notably, the decomposition of this gain reveals that fixed-geometry optimization contributes approximately 12.7%, while dynamic angle adjustment provides a further 2.1% improvement, suggesting that geometric configuration at the design stage carries greater weight than real-time actuation alone. This finding echoes observations by Jayathissa et al., who reported that module the ratio of PV width to shading device spacing and angle optimization are dominant determinants of annual photovoltaic yield in building-integrated systems [27]. In addition to the increase in photovoltaic electricity generation, the benefit of adaptive angle adjustment is also reflected in the coordinated improvement of overall façade performance, including reduced cooling energy demand, improved glare control, and better visual openness.

The 33.4% reduction in annual cooling energy consumption relative to the unshaded baseline surpasses the performance of both the fixed-angle photovoltaic façade (29.5% reduction) and photovoltaic louver shading (27.7% reduction), confirming that adaptive shading provides a meaningful thermal benefit beyond what static systems can deliver. This advantage is most pronounced during peak summer months, when the façade adopts a more compact configuration in response to high solar altitude and radiation intensity. The sUDI improvement from 0.66 in the baseline to 0.89 in the adaptive case represents a 34.8% gain, indicating that dynamic daylighting regulation substantially increases the proportion of time during which indoor illuminance falls within the useful range of 100–2000 lx. Although photovoltaic louver shading marginally outperforms the adaptive system on the single sUDI metric (0.90 vs. 0.89), this narrow advantage is offset by its inferior performance in cooling energy reduction, glare control, and visual openness, underscoring the importance of evaluating façade systems under a unified multi-objective framework rather than optimizing for any single indicator.

The sDGP range of 0.15–0.21 maintained by the adaptive façade throughout the year represents a consistently low glare risk, remaining below the commonly adopted “disturbing” threshold of 0.38 at all times. This is particularly significant during winter months, when low solar altitude angles increase direct sunlight penetration risk; the dynamic adjustment of Angle1 in response to these conditions reduces sDGP by approximately 2% relative to the fixed-angle scheme, demonstrating a clear operational benefit of real-time control. Meanwhile, the annual average OF of 0.27, consistently higher than both comparator shading schemes, confirms that the adaptive system achieves a more favorable balance between shading effectiveness and outward view preservation, which is a dimension frequently overlooked in photovoltaic façade research.

4.2. Mechanisms underlying system performance and design implications

The performance advantages observed in this study can be attributed to two interrelated mechanisms: spatially differentiated control through layered façade architecture, and temporally responsive regulation enabled by the data-driven optimization framework. The sensitivity analysis established that meteorological parameters constitute the dominant driving force for all performance objectives, while solar position parameters serve as geometric intermediaries that amplify or constrain the effect of façade configuration. Façade-related parameters, though exhibiting limited first-order effects, show substantially elevated total-order sensitivity indices, indicating that their influence is primarily realized through nonlinear interactions with environmental variables. This finding has a direct implication for design: isolated adjustment of any single panel angle or module count is unlikely to yield consistent performance gains unless coordinated with the prevailing solar and meteorological context.

The layered control architecture addresses this complexity by assigning differentiated functional roles across the vertical extent of the façade. The upper zone, subjected to more direct solar exposure, prioritizes shading intensity and photovoltaic output through smaller tilt angles and more active azimuthal deflection. The middle zone balances shading and daylighting transmission, while the lower zone maintains larger opening angles to preserve outward views and support occupant visual comfort. This spatial division of function effectively distributes conflicting objectives across distinct zones, reducing the degree of trade-off that any single layer must resolve and thereby improving the overall system's capacity for multi-objective coordination. The emergent pattern of “converging at midday and opening in the morning and late afternoon” represents a thermally and optically rational response to the diurnal solar path, and its consistency across all four representative seasons indicates that the optimization framework has successfully internalized the periodic structure of outdoor environmental variation.

4.3. Limitations and directions for future research

Despite the promising results, several limitations need to be acknowledged. First, the study relies entirely on simulation-based analysis using Typical Meteorological Year data for Shenzhen, which, while standard practice, cannot fully capture the stochastic variability of real climatic conditions or the operational uncertainties inherent in physical deployments. The power generation and control models involve idealized assumptions regarding module efficiency, mechanical actuation response time, and sensor accuracy, which may lead to an overestimation of system performance under field conditions.

In this study, the PV output model addresses non-uniform irradiance at the geometric and layer level but does not explicitly represent electrical level effects such as mismatch losses, bypass diode behavior, or string and MPPT configuration, all of which can become significant for a lamellar façade in which adjacent layers may experience substantially different irradiance. As a result, the reported annual PV generation may overestimate actual output under conditions of pronounced irradiance non-uniformity, and future work should incorporate an electrical level model to quantify this gap. Moreover, the current framework does not account for the energy consumed by the actuation system itself, which, although reported as proportionally minor in comparable dynamic façade studies, should still be quantified and incorporated into the net energy balance in future work. In addition, the proposed dual-axis and layer-by-layer adaptive façade may introduce practical challenges related to actuator deployment, mechanical complexity, long-term structural reliability, and maintenance requirements. Although the layered control strategy may help reduce control complexity compared with fully independent actuation of every unit, these engineering factors may still influence real-world performance and implementation feasibility. Therefore, future research should further examine these issues through physical prototyping, long-term operational monitoring, and life-cycle assessment.

Lastly, the study is confined to a one building typology, orientation, and climate zone, hence the generalizability of the findings should be further studied in the future. Future research should extend the validation to measured data from physical prototypes and apply the proposed framework to additional climate zones, building types, and façade orientations to assess its broader applicability.

4.4. Conclusion

This study proposes and validates a high-degree-of-freedom adaptive photovoltaic façade design and control method with hourly responsiveness for office buildings in hot summer and warm winter regions. By coupling parametric modeling, annual hourly performance evaluation, a data-driven surrogate model, and a multi-objective optimization framework, the study establishes an integrated control system that simultaneously considers photovoltaic power generation, luminous environment quality, and building energy consumption. In addition, a solution-selection strategy based on Nash game theory is adopted to improve the balance and stability of multi-objective decision-making. The results show that, compared with fixed photovoltaic louvers, the adaptive photovoltaic façade increases annual photovoltaic electricity generation by approximately 15%. Compared with the no-façade case, it reduces annual cooling energy consumption by approximately 33%. In terms of the luminous environment, the adaptive photovoltaic façade can significantly improve the level of indoor Spatial Useful Daylight Illuminance (sUDI), with an annual average sUDI of 0.89. At the same time, glare risk is maintained at a relatively low level, with an annual average spatial Daylight Glare Probability (sDGP) of approximately 0.18, while a relatively stable degree of visual openness is preserved, with an annual average OF of 0.27.

Nevertheless, several limitations should be acknowledged. The energy consumption of the actuation system itself has not been explicitly quantified within the net energy balance, electrical level effects such as mismatch losses, bypass diode behavior, or string and MPPT configuration were not fully accounted in the research. Moreover, the analysis is conducted in a representative office building setup, façade orientation, and climate zone. Hence, future research should prioritize experimental validation through physical prototypes under real operating conditions to assess the gap between simulated and measured performance. Extending the proposed framework to additional climate zones, building types, and façade orientations would further substantiate its generalizability and support broader engineering implementation. These advances would strengthen the pathway from simulation-validated concept to deployable building system, contributing to the wider adoption of adaptive photovoltaic façades as an effective technological solution for energy efficiency and indoor environmental quality in the built environment.

Declaration of generative AI and assisted technologies in the writing process

In preparing this manuscript, the authors used OpenAI's GPT-5 to improve grammar and sentence structure. The tool was not used to generate original scientific content, results, or data interpretations. After using this AI assisted service, the authors reviewed and edited the content as necessary and take full responsibility for the content of the publication.

CRediT authorship contribution statement

Sijun Liu: . **Zhaoyang Luo:** Writing – review & editing, Validation, Methodology, Formal analysis. **Xiaodong Yang:** Writing – review & editing, Resources, Formal analysis. **Yudai Liu:** Writing – review & editing, Supervision, Methodology. **Yi Zhang:** Writing – review & editing, Supervision, Data curation. **Pengyuan Shen:** Writing – review

& editing, Supervision, Resources, Project administration, Methodology, Funding acquisition, Conceptualization.

Declaration of competing interest

The authors declare that they have no known competing financial interests or personal relationships that could have appeared to influence the work reported in this paper.

Acknowledgement

This work is supported by Shenzhen Fundamental Research Program (JCYJ20250604180231041).

Appendix

Appendix I. Building simulation parameters

.

Table A1
Building simulation parameters.

System	Component	Simulation Parameter
Building Envelope	Wall	Aerated concrete, U = 1.5 W/m^2·K
	Window	Double glazing, U = 2.24 W/m^2·K
		Visible light transmittance, T_{vis} = 0.6
		Solar heat gain coefficient, SHGC = 0.48
		Window-to-wall ratio, WWR = 0.53
Shading Device	Aluminum structural component	Visible light transmittance, T_{vis} = 0.2
		Reflectance, R_{vis} = 0.47
	Photovoltaic component	Visible light transmittance, T_{vis} = 0
		Reflectance, R_{vis} = 0.05
HVAC	Cooling condition setting	Cooling setpoint = 26°C
		Cooling COP = 3.5
	Cooling setpoint schedule	01:00–06:00: 37°C; 07:00: 29°C; 08:00–18:00: 26°C; 19:00–24:00: 37°C
	Ventilation rate	Ventilation rate = 30 m^3/h per person
Internal Loads	Occupancy	Occupancy density = 0.1 person/m^2
		Radiative fraction = 0.3
		Occupancy schedule: 08:00–18:00
	Equipment	Equipment power density = 15 W/m^2
		Equipment schedule: 08:00–18:00 weekdays
	Lighting	Lighting power density = 8 W/m^2
		Target illuminance = 500 lx
Surface Properties	Interior walls	Reflectance = 0.5
	Ceiling	Reflectance = 0.8
	Floor	Reflectance = 0.2
Daylighting Simulation	Sensor setting	Height: 0.75 m above floor level
		Grid: 0.5 m × 0.5 *m*

Appendix II. Model configuration and performance comparison

.

Table A2
Hyperparameter settings for different machine learning models.

Algorithm	Hyperparameter	Search Range
Linear Regression	—	—
Lasso Regression	α	0.001, 0.01, 0.1, 1, 10
Ridge Regression	α	0.001, 0.01, 0.1, 1, 10
Elastic Net Regression	α	0.001, 0.01, 0.1, 1, 10
	l1_ratio	0.1, 0.3, 0.5, 0.7, 0.9
Polynomial Regression	Polynomial degree (n)	2, 3, 4, 5
	Regularization type	None, Ridge
	α (Ridge)	0.01, 0.1, 1
Decision Tree Regression	max_depth	3, 5, 7, 9
	min_samples_split	2, 5, 10
	min_samples_leaf	1, 3, 5
Random Forest Regression	n_estimators	200, 500, 800
	max_depth	5, 7, 9
	min_samples_leaf	1, 3, 5
	max_features	sqrt, log2
Extreme Gradient Boosting (XGBoost)	n_estimators	500, 700, 1000
	learning_rate	0.02, 0.05, 0.1, 0.15

(*continued on next page*)

Table A2 (*continued*)

Algorithm	Hyperparameter	Search Range
	max_depth	4, 7, 9
	min_child_weight	1, 3, 6
	subsample	0.5, 0.7, 0.9
	colsample_bytree	0.7, 0.9
Multilayer Perceptron (MLP)	Number of hidden layers	1, 2, 4
	Number of neurons per layer	16, 32, 64
	Learning rate	0.0001, 0.001, 0.01
	Activation function	relu, tanh
	Optimizer	Adam
	Dropout rate	0, 0.1, 0.3

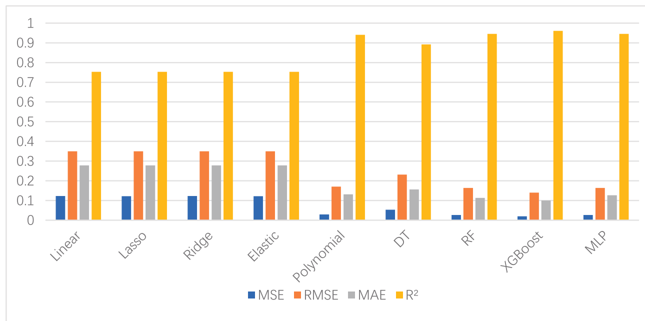

Fig. A1. Performance Comparison of Different Machine Learning Models across Evaluation Metrics

Appendix III. Five-fold cross-validation scatter plots for Façade performance indicators

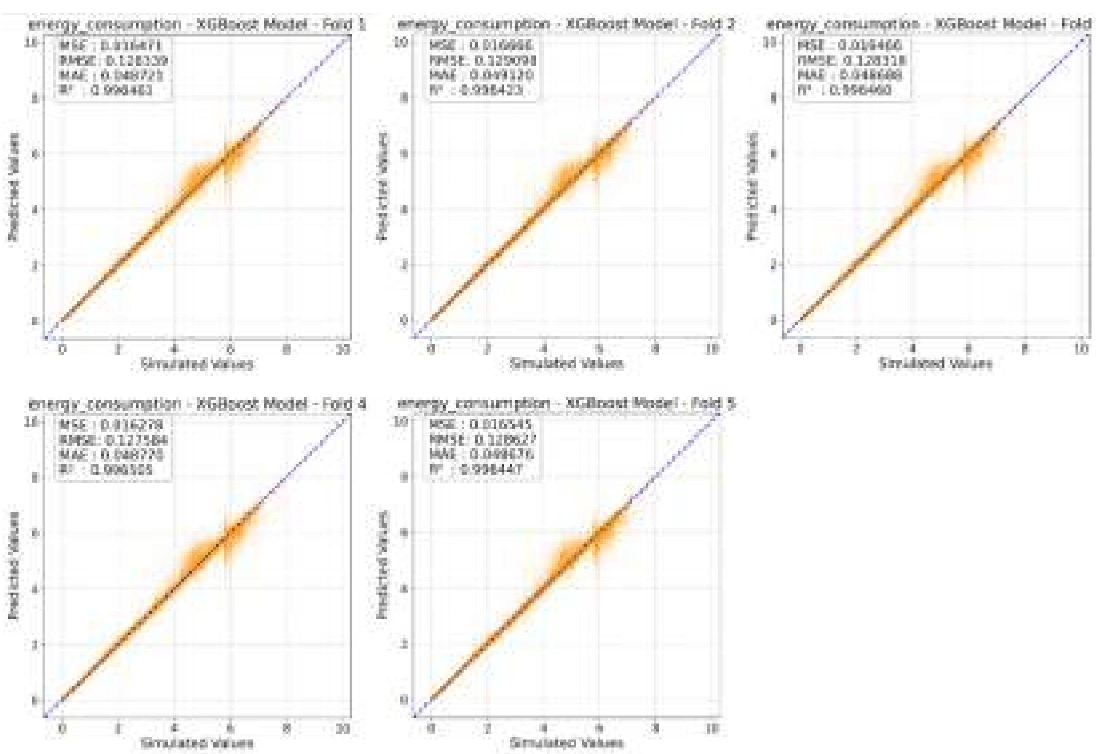

Fig. A2. Five-fold cross-validation scatter plot for cooling energy consumption

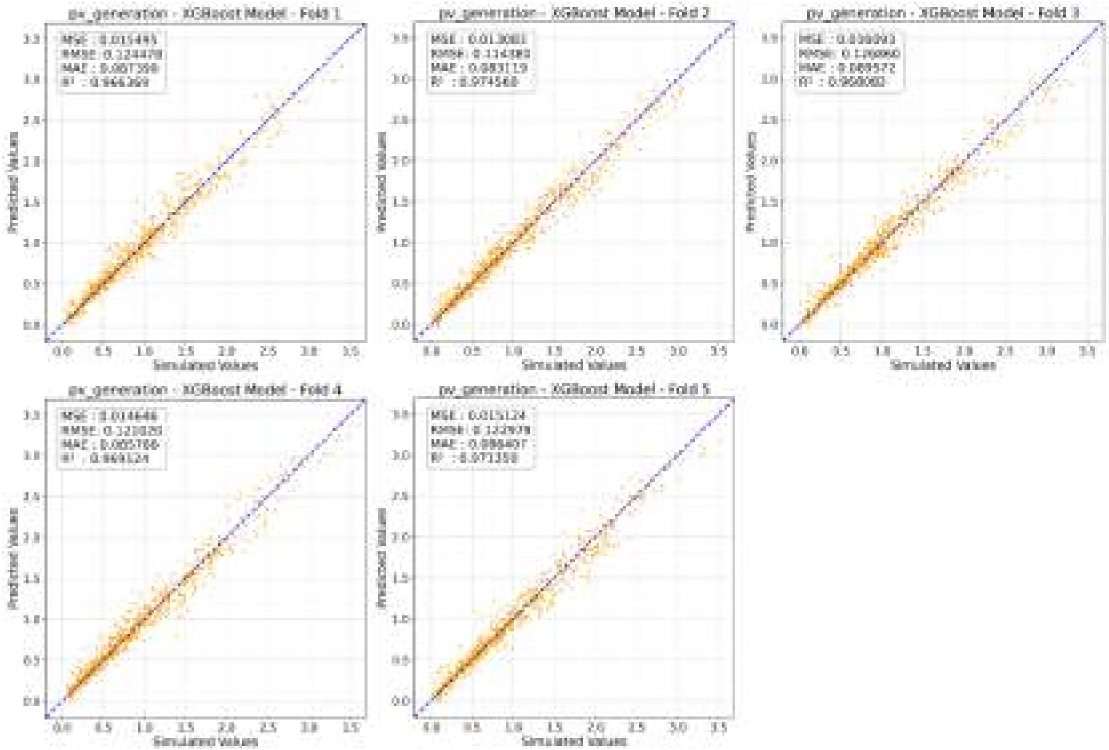

Fig. A3. Five-fold cross-validation scatter plot for photovoltaic power generation

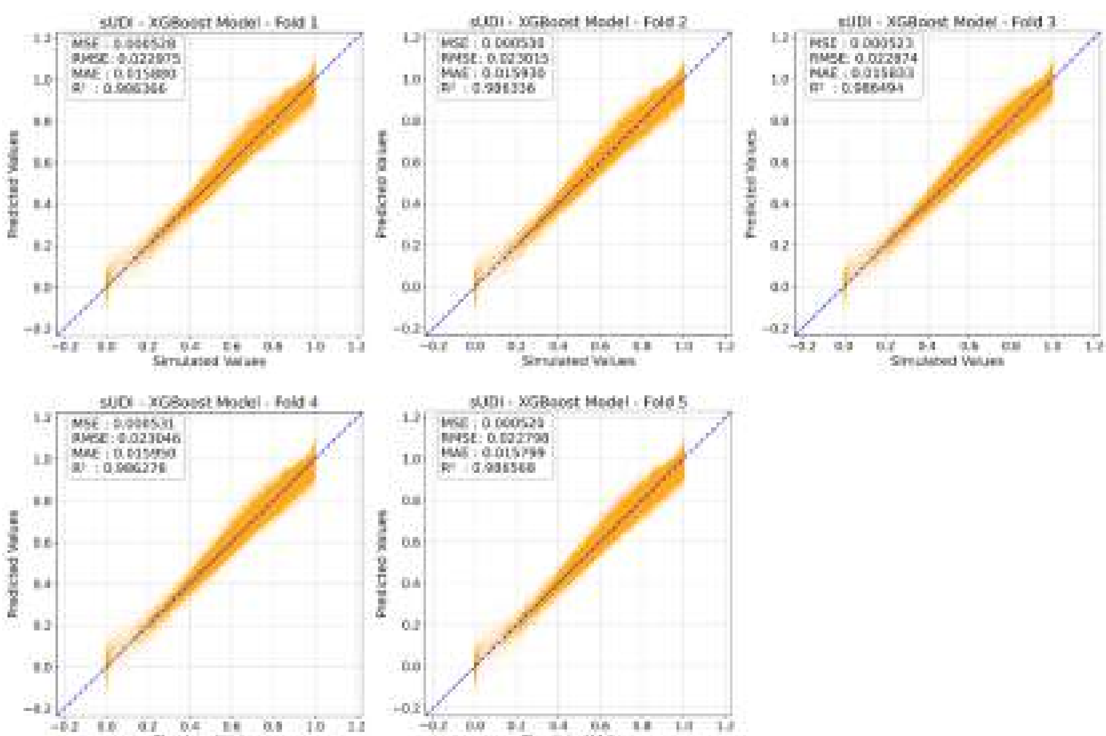

Fig. A4. Five-fold cross-validation scatter plot for sUDI

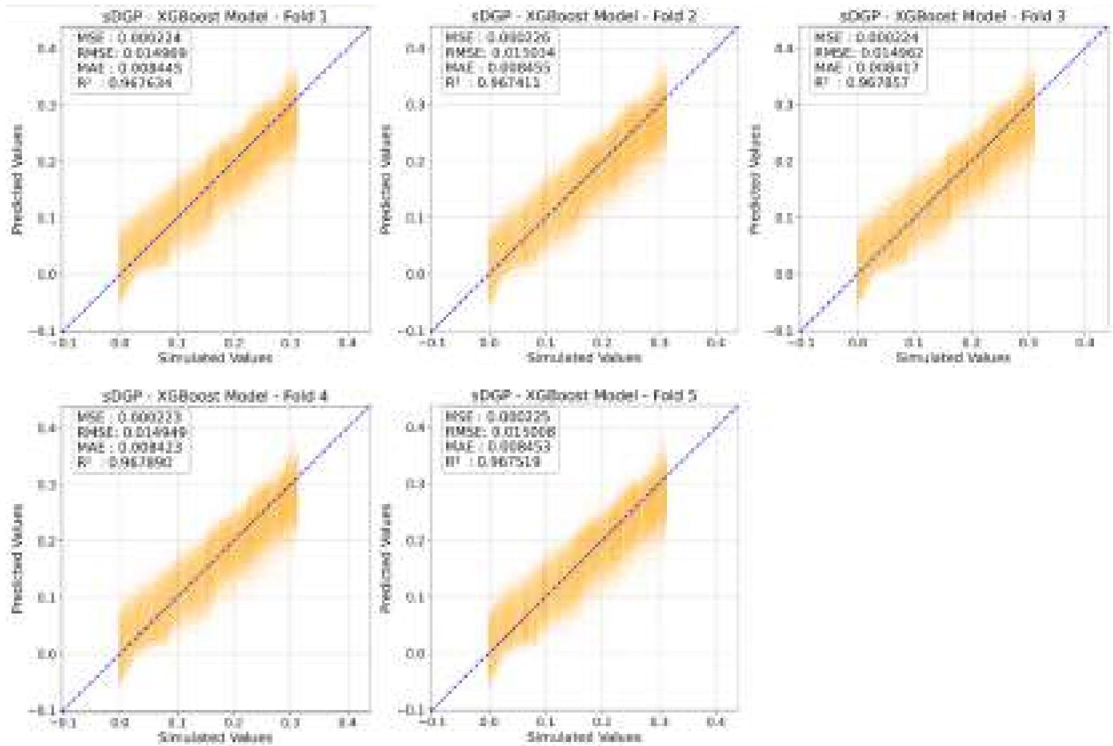

Fig. A5. Five-fold cross-validation scatter plot for sDGP

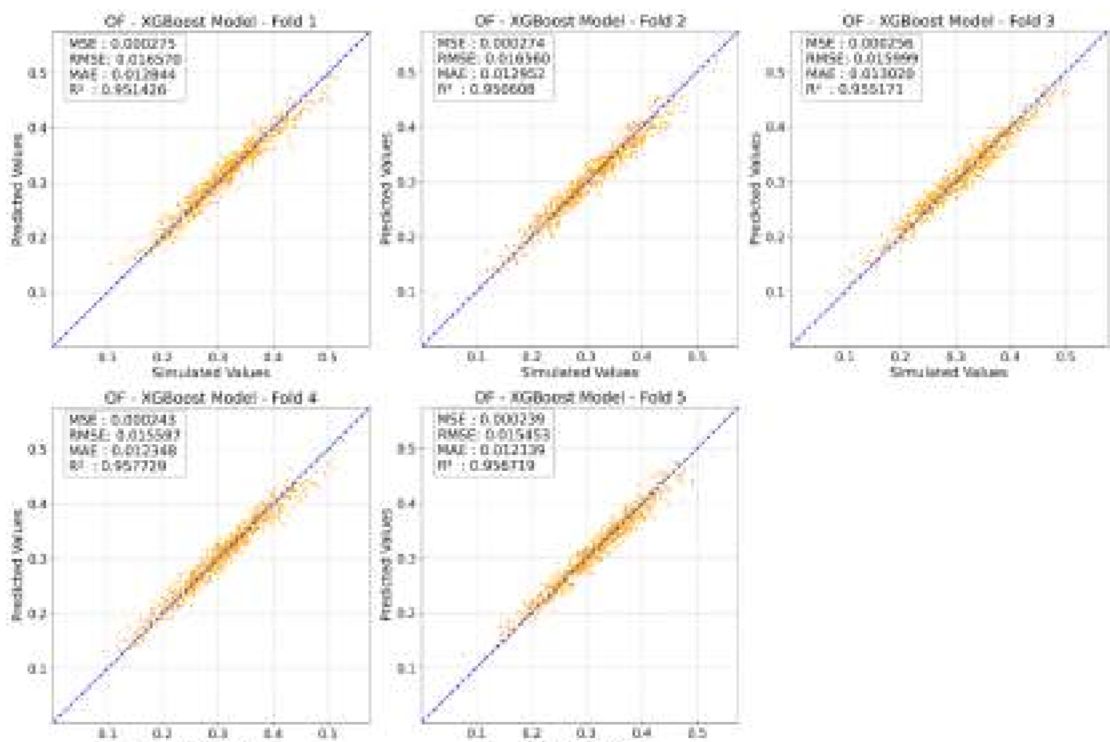

Fig. A6. Five-fold cross-validation scatter plot for OF

Appendix IV. Second-order sensitivity

To further clarify the nonlinear interactions among different parameters, second-order Sobol sensitivity analysis was introduced. The results indicate that the nonlinear behavior of the adaptive photovoltaic façade system primarily originates from the coupling between meteorological parameters and solar position parameters, as well as their synergistic amplification with photovoltaic façade parameters. Different performance objectives exhibit significant differences in dominant interaction types and spatial distributions, reflecting the diversity of system regulation mechanisms.

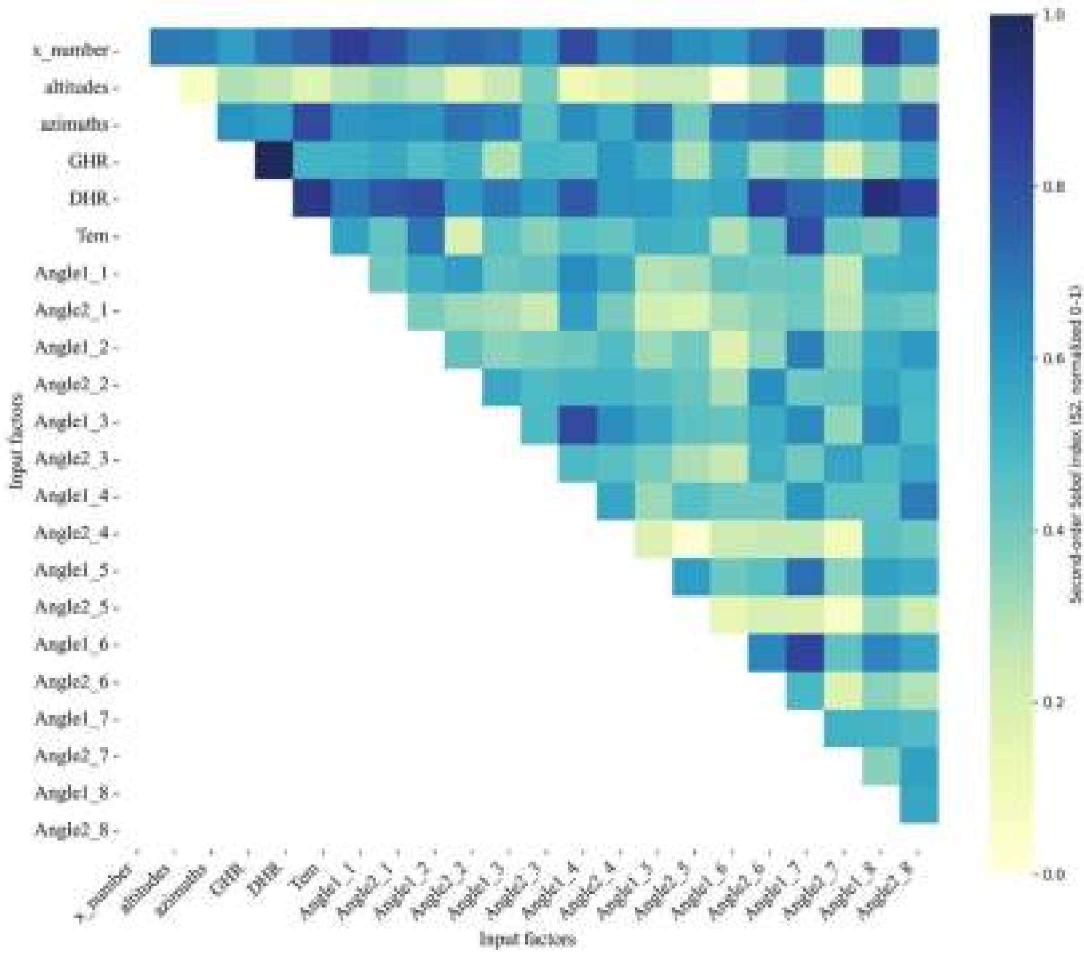

Fig. A7. Second-order Sobol sensitivity analysis of photovoltaic power generation

Fig. A7 shows that the performance variation of photovoltaic power generation is predominantly governed by meteorological parameters, with synergistic influences from solar position and photovoltaic façade parameters. Among them, the interaction between global horizontal radiation (GHR) and diffuse horizontal radiation (DHR) exhibits the highest second-order sensitivity, indicating that power output is highly sensitive to changes in radiation composition, which jointly determines the overall solar exposure conditions of the system.

In addition to radiation parameters, the photovoltaic module configuration exhibits a significant interaction amplification effect in the second-order analysis. Its interactions with solar altitude, solar azimuth, and multiple façade rotation angles form medium-to-high sensitivity regions, suggesting that module configuration indirectly affects power generation performance by regulating shading rhythms, component exposure ratios, and shadow distribution. In terms of spatial distribution, the upper and middle façade angles dominate the interactions, indicating that power generation is more sensitive to solar exposure conditions at higher façade levels.

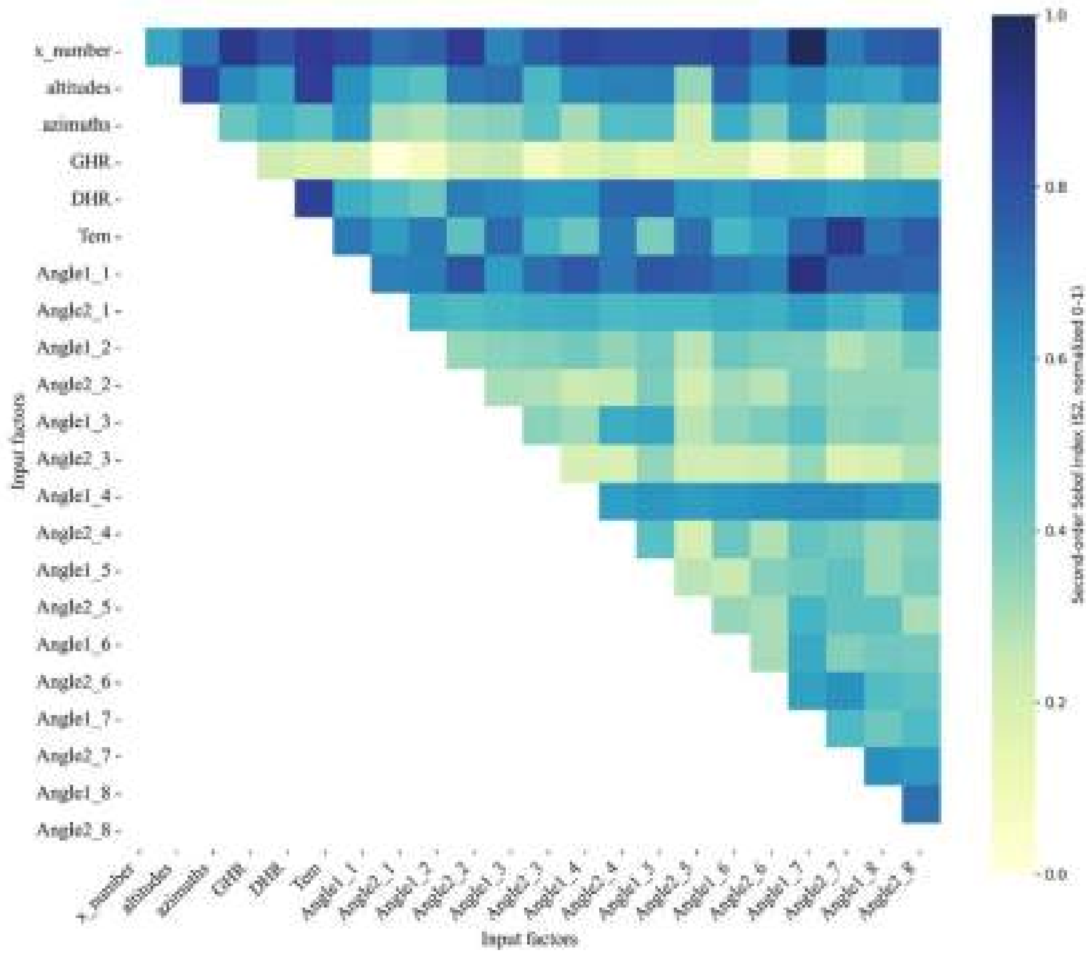

Fig. A8. Second-order Sobol sensitivity analysis of cooling energy consumption

Fig. A8 indicates that the nonlinear characteristics of cooling energy consumption mainly arise from the extensive interactions between photovoltaic module configuration and both meteorological and solar position parameters. Continuous high-sensitivity regions are observed between module configuration and solar altitude and azimuth, suggesting that module design significantly influences shading patterns and solar exposure boundaries under varying solar positions, thereby amplifying the impact of geometric regulation on cooling loads.

Among meteorological parameters, the interaction between diffuse radiation and air temperature is the most prominent, indicating a strong coupling effect of radiative and thermal environmental changes on cooling energy consumption. In contrast, the interaction contributions of façade rotation angles are generally at a moderate level, with the upper façade angles showing higher sensitivity than the middle and lower parts. This suggests that cooling loads are more responsive to geometric adjustments at the upper façade, although these are not the primary source of nonlinearity.

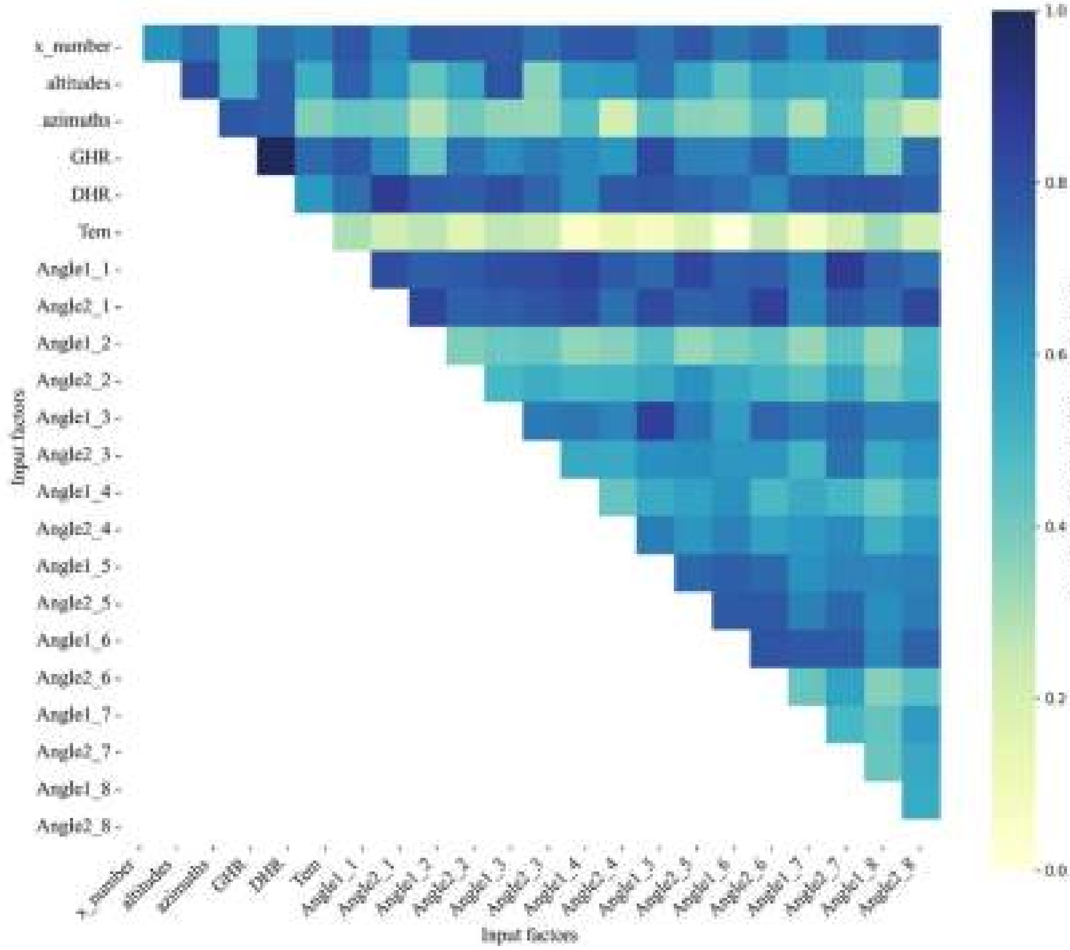

Fig. A9. Second-order Sobol sensitivity analysis of spatial Useful Daylight Illuminance (sUDI)

Fig. A9 shows that spatial Useful Daylight Illuminance (sUDI) is primarily governed by the interactions between meteorological parameters (GHR and DHR) and photovoltaic façade rotation angles. Radiation parameters and façade angles at different levels form continuous and extensive high-sensitivity regions, indicating that façade geometry can significantly regulate the formation of effective indoor daylighting ranges under varying radiation conditions.

The photovoltaic module configuration exhibits stable medium-to-high sensitivity in the second-order analysis of sUDI, suggesting that it works synergistically with radiation conditions and angular control by influencing shading patterns and daylight admission rhythms, thereby affecting daylighting stability. In terms of angular distribution, the interaction sensitivity of the upper and middle façade angles is significantly higher than that of the lower part, indicating that sUDI is more sensitive to geometric adjustments at higher façade levels, while the contribution of lower angles remains relatively limited.

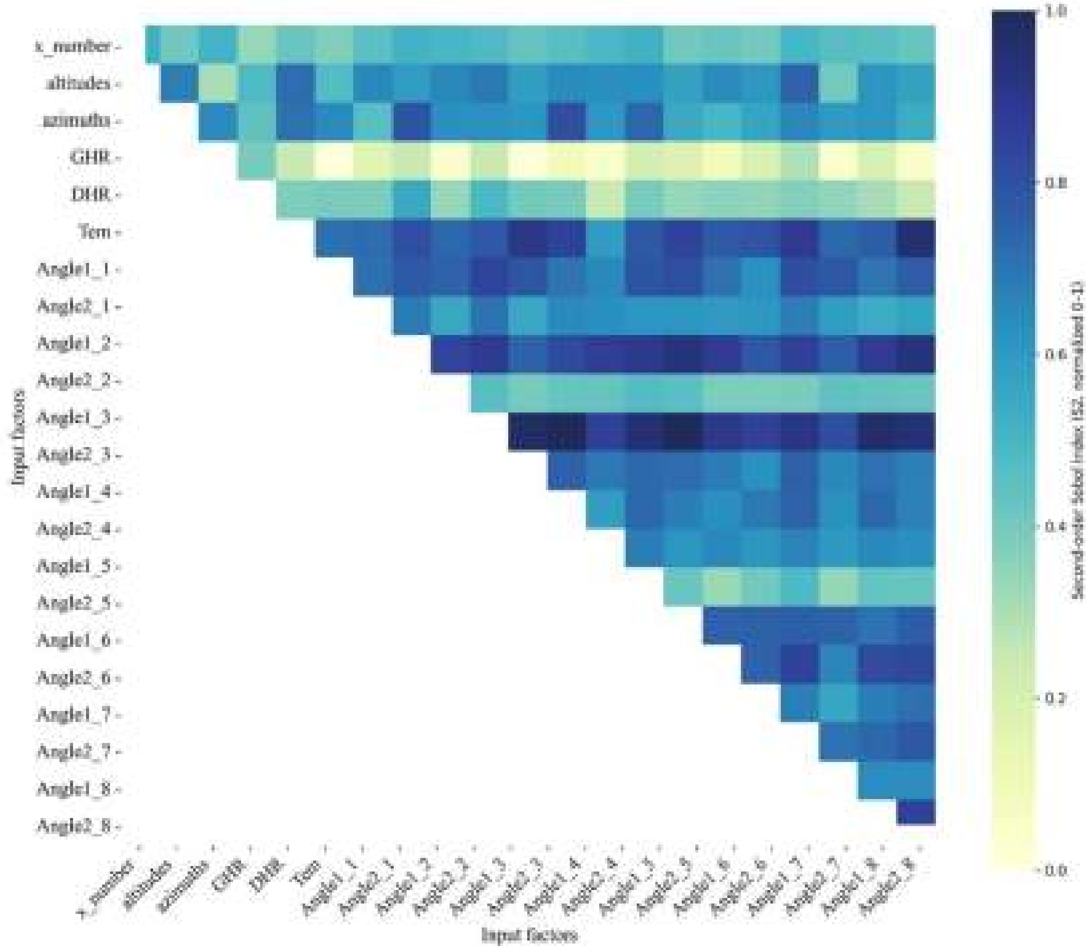

Fig. A10. Second-order Sobol sensitivity analysis of spatial Daylight Glare Probability (sDGP)

Fig. A10 indicates that the interaction between solar altitude and solar azimuth constitutes the dominant source of nonlinearity in spatial Daylight Glare Probability (sDGP). These parameters form continuous high-intensity sensitivity regions with multiple photovoltaic façade rotation angles, demonstrating that glare risk responds highly nonlinearly to variations in solar position. The façade angles, through their coupling with solar geometry, regulate the paths of direct high-intensity light and thus represent critical structural factors influencing glare probability.

In comparison, the interaction sensitivity of photovoltaic module configuration in sDGP remains at a moderate level, indicating that module variation can either mitigate or exacerbate glare to some extent, but is not the determining factor. Spatially, higher interaction sensitivity is observed in the upper and lower façade angles, corresponding respectively to high-angle direct light penetration and horizontal line-of-sight obstruction, which are key regions for glare control.

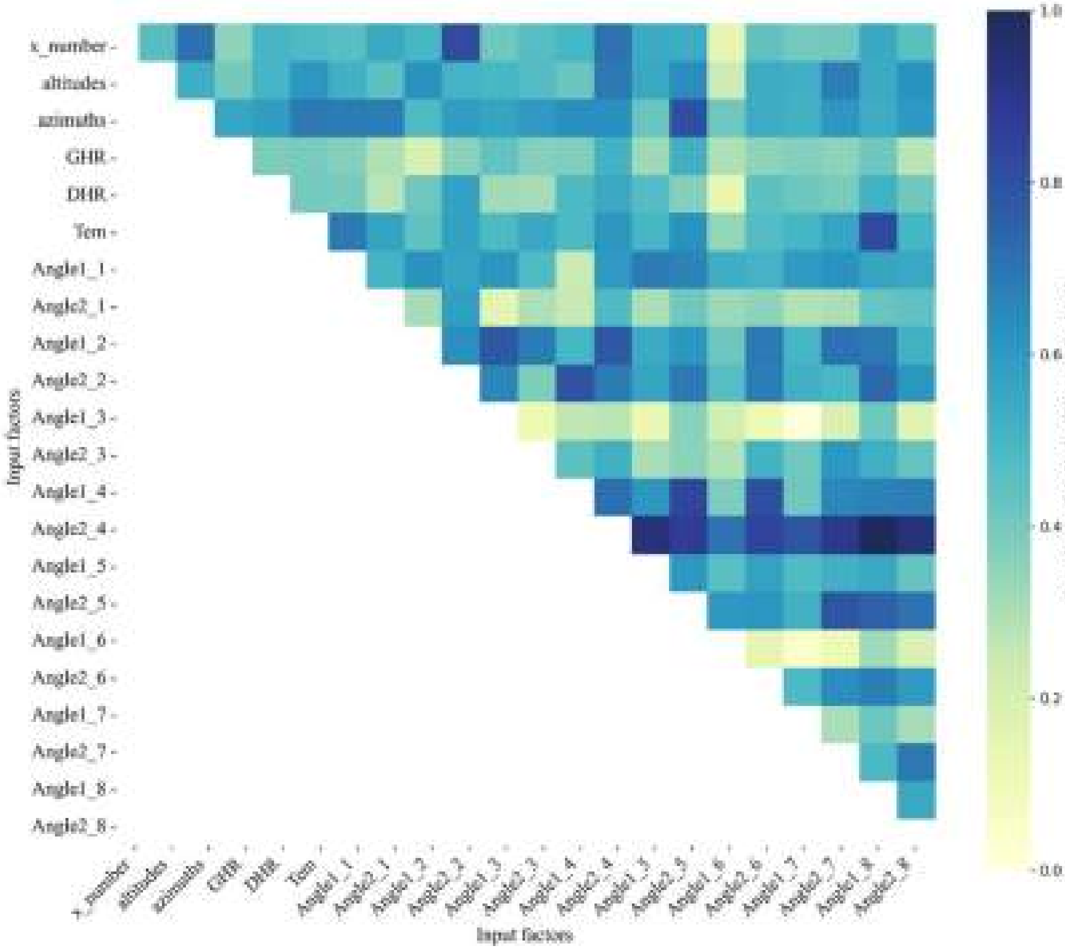

Fig. A11. Second-order Sobol sensitivity analysis of Openness Factor (OF)

Fig. A11 shows that the OF is primarily dominated by interactions among photovoltaic façade parameters, with relatively weak sensitivity to meteorological and solar position parameters. The photovoltaic module configuration demonstrates a significant interaction amplification effect, indicating that it influences indoor visual openness by modifying shading repetition patterns and working in conjunction with façade rotation angles.

Among angular parameters, the middle and lower façade angles play a dominant role, suggesting that geometric variations in these regions are most critical to visual openness. In contrast, the interaction contribution of upper façade angles is relatively limited, as their shading variations have less impact on primary indoor viewing directions. These findings indicate that OF is more strongly constrained by internal geometric configurations rather than driven by external environmental conditions.

Data availability

Data will be made available on request.

References

[1] F. Tahmasbi, A.I. Khdair, G.A. Aburumman, M. Tahmasebi, N.H. Thi, M. Afrand, Energy-efficient building façades: a comprehensive review of innovative technologies and sustainable strategies, J. Build. Eng. 99 (2025) 111643, https://doi.org/10.1016/j.jobe.2024.111643.

[2] Z. Liu, Q. Zhou, Z. Tian, B. He, G. Jin, A comprehensive analysis on definitions, development, and policies of nearly zero energy buildings in China, Renew. Sustain. Energy Rev. 114 (2019) 109314, https://doi.org/10.1016/j.rser.2019.109314.

[3] P. Shen, Z. Wang, Y. Ji, Exploring potential for residential energy saving in New York using developed lightweight prototypical building models based on survey data in the past decades, Sustain. Cities Soc. 66 (2021) 102659, https://doi.org/10.1016/j.scs.2020.102659.

[4] J.J. Wang, J. Xu, An unplanned commercial district in a fast-growing city: a case study of Shenzhen, China, J. Retail. Consum. Serv. 9 (2002) 317–326, https://doi.org/10.1016/S0969-6989(02)00002-4.

[5] N. Nasrollahzadeh, Comprehensive building envelope optimization: improving energy, daylight, and thermal comfort performance of the dwelling unit, Journal of Building Engineering 44 (2021) 103418, https://doi.org/10.1016/j.jobe.2021.103418.

[6] M. González-Torres, L. Pérez-Lombard, J.F. Coronel, I.R. Maestre, D. Yan, A review on buildings energy information: Trends, end-uses, fuels and drivers, Energy Rep. 8 (2022) 626–637, https://doi.org/10.1016/j.egyr.2021.11.280.

[7] R.C.G.M. Loonen, M. Trčka, D. Cóstola, J.L.M. Hensen, Climate adaptive building shells: State-of-the-art and future challenges, Renew. Sustain. Energy Rev. 25 (2013) 483–493, https://doi.org/10.1016/j.rser.2013.04.016.

[8] A. Tabadkani, A. Roetzel, H.X. Li, A. Tsangrassoulis, Design approaches and typologies of adaptive facades: a review, Autom. Constr. 121 (2021) 103450, https://doi.org/10.1016/j.autcon.2020.103450.

[9] G. Salvalai, F. Zhao, Active prefabricated façade with building-integrated photovoltaic (APF-BIPV) technologies for high energy efficient building renovation: a systematic review of recent research advancements, Energ. Buildings 348 (2025) 116440, https://doi.org/10.1016/j.enbuild.2025.116440.

[10] D. Aelenei, L. Aelenei, C.P. Vieira, Adaptive façade: concept, applications, research questions, Energy Procedia 91 (2016) 269–275, https://doi.org/10.1016/j.egypro.2016.06.218.

[11] D.S. Pillai, V. Shabunko, A. Krishna, A comprehensive review on building integrated photovoltaic systems: Emphasis to technological advancements, outdoor

testing, and predictive maintenance, Renew. Sustain. Energy Rev. 156 (2022) 111946, https://doi.org/10.1016/j.rser.2021.111946.
[12] Y.-J. Jun, T.-G. Han, Y.-H. Song, K.-S. Park, A study on the enhancement of energy efficiency and indoor environment through the integration of solar photovoltaic modules in daylighting louver systems, Sol. Energy 282 (2024) 112931, https://doi.org/10.1016/j.solener.2024.112931.
[13] S. Sadatifar, E. Hannoufa, E. Johlin, Design of multi-objective optimized dynamic photovoltaic shades and thin films, Sol. Energy 278 (2024) 112759, https://doi.org/10.1016/j.solener.2024.112759.
[14] Y. Zou, Y. Deng, D. Xia, S. Lou, X. Yang, Y. Huang, J. Guo, Z. Zhong, Comprehensive analysis on the energy resilience performance of urban residential sector in hot-humid area of China under climate change, Sustain. Cities Soc. 88 (2023) 104233, https://doi.org/10.1016/j.scs.2022.104233.
[15] H. Tang, X. Chai, W. Jing, Y. Li, C. Li, Assessment of photovoltaic power generation and radiative cooling potentials in old residential districts: a case study of Shenzhen, Energ. Buildings 319 (2024) 114493, https://doi.org/10.1016/j.enbuild.2024.114493.
[16] Z. Nagy, B. Svetozarevic, P. Jayathissa, M. Begle, J. Hofer, G. Lydon, A. Willmann, A. Schlueter, The Adaptive Solar Facade: from concept to prototypes, Front. Archit. Res. 5 (2016) 143–156, https://doi.org/10.1016/j.foar.2016.03.002.
[17] E.S. Mazzucchelli, M. Alston, M. Brzezicki, L. Doniacovo, Study of a BIPV adaptive system: combining timber and photovoltaic technologies, J. Facade Des. Eng. 6 (2018) 149–162.
[18] A. Monteleone, G. Rodonò, A. Gagliano, V. Sapienza, SLICE: an innovative photovoltaic solution for adaptive envelope prototyping and testing in a relevant environment, Sustainability 13 (2021) 8701.
[19] Y. Zheng, J. Wu, H. Zhang, C. Lin, Y. Li, X. Cui, P. Shen, A novel sun-shading design for indoor visual comfort and energy saving in typical office space in Shenzhen, Energ. Buildings 328 (2025) 115083, https://doi.org/10.1016/j.enbuild.2024.115083.
[20] M. Brzezicki, P. Regucki, J. Kasperski, Optimization of useful daylight illuminance for vertical shading fins covered by photovoltaic panels for a case study of an office room in the city of Wroclaw, Poland, Buildings 11 (2021) 637.
[21] W. Zou, Y. Wang, E. Tian, J. Wei, J. Peng, J. Mo, A new dynamic and vertical photovoltaic integrated building envelope for high-rise glaze-facade buildings, Engineering 39 (2024) 194–203, https://doi.org/10.1016/j.eng.2024.01.014.
[22] H.S. Choi, Kinetic photovoltaic facade system based on a parametric design for application in signal box buildings in Switzerland, Appl. Sci. 13 (2023) 4633.
[23] A. Ożadowicz, G. Walczyk, Energy performance and control strategy for dynamic façade with perovskite PV panels—technical analysis and case study, Energies 16 (2023) 3793, https://doi.org/10.3390/en16093793.
[24] Y.B. Assoa, J. Ratovonkery, C. Ménézo, R. Morlot, Towards a bio-inspired design of a photovoltaic facade, Renew. Energy 229 (2024) 120679, https://doi.org/10.1016/j.renene.2024.120679.
[25] S. Jalali, E. Nicoletti, L. Badarnah, From flora to solar adaptive facades: integrating plant-inspired design with photovoltaic technologies, Sustainability 16 (2024) 1145.
[26] H. Mousazadeh, A. Keyhani, A. Javadi, H. Mobli, K. Abrinia, A. Sharifi, A review of principle and sun-tracking methods for maximizing solar systems output, Renew. Sustain. Energy Rev. 13 (2009) 1800–1818, https://doi.org/10.1016/j.rser.2009.01.022.
[27] P. Jayathissa, Optimising building net energy demand with dynamic BIPV shading, Appl. Energy 202 (2017) 726–735.
[28] B. Svetozarevic, M. Begle, P. Jayathissa, S. Caranovic, R.F. Shepherd, Z. Nagy, I. Hischier, J. Hofer, A. Schlueter, Dynamic photovoltaic building envelopes for adaptive energy and comfort management, Nat. Energy 4 (2019) 671–682, https://doi.org/10.1038/s41560-019-0424-0.
[29] Y. Gao, A photovoltaic window with sun-tracking shading elements towards maximum power generation and non-glare daylighting, Appl. Energy 228 (2018) 1454–1472.
[30] X. Liang, H. Zhang, B. Sun, Parametric design of photovoltaic louver integrated shading devices for west facade windows of office buildings in central China, J. Asian Architect. Build. Eng. 23 (2024) 1–15, https://doi.org/10.1080/13467581.2024.2320326.
[31] N. Biloria, M. Makki, N. Abdollahzadeh, Multi-performative façade systems: the case of real-time adaptive BIPV shading systems to enhance energy generation potential and visual comfort, Front. Built Environ. 9 (2023) 1119696, https://doi.org/10.3389/fbuil.2023.1119696.
[32] S. Miraba, A. Salehi, M. Rostamzadeh-Renani, R. Ehteshami, A. Shahbazi, R. Rostamzadeh-Renani, S.A.H.H. Dehkordi, M. Baghoolizadeh, Adaptive BIPV shading optimization for electricity generation and building electricity management, sDA, and DGP using multi-objective algorithms, Appl. Energy 402 (2025) 126860, https://doi.org/10.1016/j.apenergy.2025.126860.
[33] S. Tharushi Imalka, R.J. Yang, Y. Zhao, Machine learning driven building integrated photovoltaic (BIPV) envelope design optimization, Energy Build. 324 (2024) 114882, https://doi.org/10.1016/j.enbuild.2024.114882.
[34] H. Qiu, Z. Ma, Y. Hu, D. Wu, L. Zhang, G. He, Multi-performance prediction and optimization for building-integrated photovoltaics facades with passive design via explainable machine learning, Sol. Energy 301 (2025) 113871, https://doi.org/10.1016/j.solener.2025.113871.
[35] S. Yeon, B. Yu, B. Seo, Y. Yoon, K.H. Lee, ANN based automatic slat angle control of venetian blind for minimized total load in an office building, Sol. Energy 180 (2019) 133–145, https://doi.org/10.1016/j.solener.2019.01.027.
[36] J. Xie, A.O. Sawyer, Simulation-assisted data-driven method for glare control with automated shading systems in office buildings, Build. Environ. 196 (2021) 107801, https://doi.org/10.1016/j.buildenv.2021.107801.
[37] Z. Luo, Key control variables affecting interior visual comfort for automated louver control in open-plan offices—A study using machine learning, Build. Environ. 207 (2022) 108565.
[38] M. Takhmasib, Machine-learned kinetic Façade: Construction and artificial intelligence enabled predictive control for visual comfort, Autom. Constr. 156 (2023) 105093.
[39] M. Wang, Z. Jia, C. Xiang, Machine learning-based adaptive control of PV shading for residential energy and visual comfort optimization, Build. Environ. 283 (2025) 113359, https://doi.org/10.1016/j.buildenv.2025.113359.
[40] B. Wang, Y. Xu, H. Wang, X. Zhang, Y. Chen, R. Tang, A. Yan, M. Zhang, Y. He, Utilizing a three-zone control model of adaptive concentrating photovoltaic facade to enhance visual comfort and energy benefits, Energ. Buildings 345 (2025) 116125, https://doi.org/10.1016/j.enbuild.2025.116125.
[41] J. Hu, X. Zheng, J. Lu, W. Chen, P. Beccarelli, S. Huang, Y. Xu, X. Qi, J. Zhang, Y. Liu, W. Guo, Experimental evaluation of louver-integrated photovoltaic windows for high-rise building facades, Energ. Buildings 349 (2025) 116475, https://doi.org/10.1016/j.enbuild.2025.116475.
[42] S. Chen, L. Zhao, L. Zheng, G. Bi, A rapid evaluation method for design strategies of high-rise office buildings achieving nearly zero energy in Guangzhou, J. Build. Eng. 44 (2021) 103297, https://doi.org/10.1016/j.jobe.2021.103297.
[43] P. Jayathissa, M. Luzzatto, J. Schmidli, J. Hofer, Z. Nagy, A. Schlueter, Optimising building net energy demand with dynamic BIPV shading, Appl. Energy 202 (2017) 726–735, https://doi.org/10.1016/j.apenergy.2017.05.083.
[44] H. Wilson, F. Frontini, P. Bonomo, Multi-dimensional evaluation of BIPV installations: development of a tool to assess the performance as building component and electricity generator, Energ. Buildings 312 (2024) 114207, https://doi.org/10.1016/j.enbuild.2024.114207.
[45] J.A. Duffie, W.A. Beckman, N. Blair, Solar Engineering of thermal Processes, Photovoltaics and Wind, 1st ed.,, Wiley, 2020, 10.1002/9781119540328.
[46] R. Singh, I.J. Lazarus, V.V.N. Kishore, Effect of internal woven roller shade and glazing on the energy and daylighting performances of an office building in the cold climate of Shillong, Appl. Energy 159 (2015) 317–333, https://doi.org/10.1016/j.apenergy.2015.09.009.
[47] M.G. Figueiro, B. Steverson, J. Heerwagen, K. Kampschroer, C.M. Hunter, K. Gonzales, B. Plitnick, M.S. Rea, The impact of daytime light exposures on sleep and mood in office workers, Sleep Health 3 (2017) 204–215, https://doi.org/10.1016/j.sleh.2017.03.005.
[48] A. Nabil, J. Mardaljevic, Useful daylight illuminances: a replacement for daylight factors, Energ. Buildings 38 (2006) 905–913, https://doi.org/10.1016/j.enbuild.2006.03.013.
[49] P. Theodoropoulou, E. Brembilla, R. Schipper, C. Louter, Glare-based control strategy for venetian blinds in a mixed-use conference space with fully glazed façades, J. Build. Eng. 82 (2024) 108181, https://doi.org/10.1016/j.jobe.2023.108181.
[50] G. Quek, J. Wienold, M.S. Khanie, E. Erell, E. Kaftan, A. Tzempelikos, I. Konstantzos, J. Christoffersen, T. Kuhn, M. Andersen, Comparing performance of discomfort glare metrics in high and low adaptation levels, Build. Environ. 206 (2021) 108335, https://doi.org/10.1016/j.buildenv.2021.108335.
[51] A. Jamrozik, N. Clements, S.S. Hasan, J. Zhao, R. Zhang, C. Campanella, V. Loftness, P. Porter, S. Ly, S. Wang, B. Bauer, Access to daylight and view in an office improves cognitive performance and satisfaction and reduces eyestrain: a controlled crossover study, Build. Environ. 165 (2019) 106379, https://doi.org/10.1016/j.buildenv.2019.106379.
[52] T. Zhu, Y. Yang, S. Bao, H. Raza, House price prediction using XG-boost grid search and cross-validation methods, in: D. Vlachos (Ed.), Mathematical Modeling in Physical Sciences, Springer Nature Switzerland, Cham, 2024, pp. 637–647, https://doi.org/10.1007/978-3-031-52965-8_47.
[53] F. Pianosi, K. Beven, J. Freer, J.W. Hall, J. Rougier, D.B. Stephenson, T. Wagener, Sensitivity analysis of environmental models: a systematic review with practical workflow, Environ. Model. Software 79 (2016) 214–232, https://doi.org/10.1016/j.envsoft.2016.02.008.
[54] K. Deb, A. Pratap, S. Agarwal, T. Meyarivan, A fast and elitist multiobjective genetic algorithm: NSGA-II, IEEE Trans. Evol. Comput. 6 (2002) 182–197, https://doi.org/10.1109/4235.996017.
[55] J.F. Nash, The bargaining problem, Econometrica 18 (1950) 155–162, https://doi.org/10.2307/1907266.